Comparison of the $U^{K'}_{37}$, LDI, TEX^{H}_{86} and RI-OH temperature proxies in the northern shelf of the South China Sea

Bingbing Wei[1, 2], Guodong Jia[1], Jens Hefter[2], Manyu Kang[1], Eunmi Park[2, 3, 4] and Gesine Mollenhauer [2, 3, 4]

[1]State Key Laboratory of Marine Geology, Tongji University, Shanghai, 200092, China
[2]Alfred Wegener Institute, Helmholtz Center for Polar and Marine Sciences, Bremerhaven, 27570, Germany
[3]Department of Geosciences, University of Bremen, Bremen, 28359, Germany
[4]MARUM, Center for Marine Environmental Sciences, University of Bremen, Bremen, 28359, Germany

Correspondence to: Guodong Jia (jiagd@tongji.edu.cn), Gesine Mollenhauer (gesine.mollenhauer@awi.de)

Abstract. The temperature proxies $U^{K'}_{37}$, LDI, TEX^{H}_{86} and RI-OH are derived from lipid biomarkers, namely long-chain alkenones from coccolithophorids, long-chain diols ascribed tentatively to eustigmatophytes, glycerol dialkyl glycerol tetraethers (GDGTs) and OH-GDGTs produced by Archaea, respectively. The applicability of these proxies has been examined in the South China Sea (SCS), but only one or two of them were studied in each work. Thereby, it is difficult to make a direct comparison between these temperature proxies. In this study, we investigated the above 4 proxies in the same set of surface sediment samples in the northern SCS shelf and related them to local sea surface temperature (SST), which allowed us to assess whether they represent certain seasons or are impaired by terrestrial influences, as well as to infer the preferred habitats of their source organisms. Terrestrial organic inputs appeared to have an impact on LDI, TEX^{H}_{86} and RI-OH proxies near the coast and lead to colder LDI and TEX^{H}_{86} derived temperatures, but a warmer RI-OH estimate. After excluding samples influenced by terrestrial organic input, we found that LDI-derived temperature agreed well with annual SST, while $U^{K'}_{37}$, TEX^{H}_{86} and RI-OH indices reflected mainly spring, winter and summer, respectively. The differential seasonal biases of these biomarker-derived temperatures observed here suggest that each biomarker's source organism responds differently to regional marine environmental changes in an annual cycle. Specifically, marine eustigmatophytes are likely insensitive to nutrient variations and hence show the lowest seasonal variations, while coccolithophorids could have bloomed in late spring, when nutrient inputs by freshwater are usually highest. GDGT-producing planktonic archaea likely thrive in winter, when conditions are favorable, although not clearly known, such as relatively high nutrients levels, low light, and high concentrations of SPM in the upper water due to the enhancement of vertical mixing driven by a combination of surface cooling and strong winter monsoon winds. However, OH-GDGTs likely originate from a different archaeal community, which mainly dewells in summer.

1 Introduction

Over the past three decades, organic proxies have been successfully applied to reconstruct the Quaternary or even Cenozoic temperature history of the Earth's surface ocean. The two most widely used proxies are the $U^{K'}_{37}$ from alkenones (Brassell et al., 1986) and the TEX_{86} based on archaeal isoprenoid tetraethers (Schouten et al., 2002). More recently, two additional organic thermometers, the LDI (long chain diol index) and RI-OH (ring index of hydroxylated isoprenoid glycerol dialkyl glycerol tetraethers (OH-GDGTs)), have been proposed by Rampen et al. (2007) and Lü et al. (2015).

The $U^{K'}_{37}$ proxy is based on the unsaturation of C_{37}-alkenones that are synthesized by a very restricted group of haptophyte algae, most notably the coccolithophores *Emiliania huxleyi* and *Gephyrocapsa oceanica* in typical marine environments (Farrimond et al., 1986; Volkman and L, 1995). Haptophyte algae are light-dependent and live near the sea surface with a competitive advantage in phosphorous-limited environments (Müller et al., 1998; Paasche, 2002). The TEX_{86}, as well as its modified versions TEX^{H}_{86} and TEX^{L}_{86} (Kim et al., 2010), is based on the relative abundance of isoprenoid glycerol dialkyl glycerol tetraethers (iGDGTs) containing 0–3 cyclopentane moieties (GDGT-0, 1, 2, 3, respectively) or 4 cyclopentane moieties with an additional cyclohexane moiety (crenarchaeol and its isomer, Cren and Cren'), produced by marine planktonic Thaumarchaeota (Schouten et al., 2013). Thaumarchaeota play an important role in pelagic ammonia oxidation in marine environments, and tend to maximize in abundance at subsurface depths <200 m (Schouten et al., 2013). The LDI index is derived from the long-chain diols (LCDs), the producers of which, albeit not fully clear yet, likely are eustigmatophyte algae in marine environments (Rampen et al., 2007, 2014a). Comparatively, little is known about the biological sources of OH-GDGTs and their influence on the RI-OH proxy. Culture studies suggest that Thaumarchaeota Group 1.1a (e.g., *Nitrosopumilus maritimus*) (Elling et al., 2014, 2015, 2017; Lipp and Hinrichs, 2009; Liu et al., 2012b), SAGMCG-1 (e.g., *Nitrosotalea devanaterra*) (Elling et al., 2017), and a strain of thermophilic euryarchaeota *Methanothermococcus thermolithotrophicus* could synthesize OH-GDGTs (Liu et al., 2012b).

Due to the distinctive ecology of their source organisms (e.g., depth habitat and seasonal bloom), the temperature signals from these biologically derived proxies may differ substantially between each other. For instance, in the basin of the South China Sea (SCS), the $U^{K'}_{37}$ and TEX^{H}_{86} indices likely reflect temperatures of the mixed layer (<30 m) and the subsurface (30–125 m), respectively (Jia et al., 2012). However, in the shallow coastal area of the SCS, the $U^{K'}_{37}$-derived SST estimates are biased toward the spring and summer temperatures, but those based on TEX^{H}_{86} toward the winter temperature, likely due to different blooming times (Zhang et al., 2013). By contrast, in the East China Sea (ECS), both TEX^{H}_{86} and RI-OH signals are summer biased (Lü et al., 2014, 2019; Zhang et al., 2017). Lopes et al. (2013) compared the $U^{K'}_{37}$, TEX^{H}_{86} and LDI indices in sediments from offshore southeast Australia, and found that LDI-derived temperature compares well with the temperatures of the warmest month, TEX^{H}_{86} with the temperatures of the coolest month and $U^{K'}_{37}$ with mean annual temperature. In the Australian southern and eastern coasts, $U^{K'}_{37}$ and LDI provide better estimates of winter temperature at the surface, and TEX^{H}_{86} matches well with annual temperature within 75–100 m (Smith et al., 2013).

The accuracy of organic thermometers is also prone to be interfered by the diverse origins of related biomarkers. For example, the noncalcifying haptophyte genera *Isochrysis galbana* and *Chrysotila lamellose*, are predominantly restricted to non-marine and marginal settings and expected to produce distinctly different alkenone records, which are likely to "contaminate" the $U^{K'}_{37}$ signal in marginal seas (Bijma et al., 2001). GDGTs synthesized by soil archaea and marine Euryarchaeota are likely different in composition from those produced by marine Thaumarchaeota, which could introduce biases to TEX_{86} values in conditions with inputs of archaeal lipids from multiple sources (Schouten et al., 2013; Turich et al., 2007; Weijers et al., 2006). Recently, the LDI proxy was found to be limited by the input of 1,13 and 1,15-diols from fresh-water eustigmatophyte algae, especially in the coastal seas (Balzano et al., 2018; de Bar et al., 2016; He et al. 2020). Similarly, OH-GDGTs may occur also in terrestrial environments including rivers (Chen et al., 2016; Kang et al., 2017), lakes (Liu et al., 2012a) and soils (Kang et al., 2017), which could also bias the RI-OH index in marginal seas. Nevertheless, environmental and physical parameters may also bias these proxies, including: (1) lateral advection (Benthien and Müller, 2000; Kim et al., 2009); (2) different resistance to degradation (Goni et al., 2001; Kim et al., 2009); (3) nutrient stress and light limitation (Hurley et al., 2016; Park et al., 2019; Prahl et al., 2003; Versteegh et al., 2001).

Coastal seas are an ideal place for evaluation of the influences on the organic temperature proxies of various confounding factors, due to its environmental and ecological seasonality and transition from the land to the deep-sea. In this study, we analysed alkenones, LCDs and GDGTs in surface sediments from the northern SCS shelf. $U^{K'}_{37}$, TEX^{H}_{86}, LDI and RI-OH indices have been studied in this area (Chen et al., 2018; Ge et al., 2013; Jia et al., 2017, 2012; Wei et al., 2011; Zhang et al., 2013; Zhu et al., 2018). However, only one or two of them were studied in each work. Thereby, it is difficult to make a direct comparison between them. Here, we investigated all of the above 4 temperature proxies in the same surface sediment samples and evaluated their applicability as water temperature indicators. This effort would benefit regional multi-proxy sea temperature reconstructions, which could be more comprehensive and objective than those based on any single ones (Eglinton and Eglinton, 2008). In addition, such kind of investigation can shed light on the ecology of the related biomarker producers in this region, which is not entirely understood at present.

2 Material and methods

2.1 Study area and sample collection

The Pearl River estuary (PRE) and the northern shelf of SCS lie in a (sub)tropical monsoon climate region, with strong northeasterly winds in winter and weak southwesterly winds in summer (Liu and Xie, 1999). As a result, coastal currents flow southwestward in winter (Fig. 1b), causing a strong vertical mixing and an inshore-offshore temperature gradient, while in summer, coastal currents reverse direction, except for one, which was near the western coast of the Pearl River (PR) and flow southwestward due to the large outflow of the PR (Fig. 1c, Liu and Xie, 1999; Su, 2004).

In the study area, a total of 23 core-top sediments (0–1 or 0–2 cm depths) were collected from the PRE and the coastal northern SCS, from water depths (WD) ranging from 6.5 to 1307 m (Suppl. Table 1). The samples were collected using a gravity box corer or grab sampler and then frozen at −20 °C in the laboratory before treatment.

2.2 Lipid extraction and separation

After being freeze-dried and homogenized, about 5 g of sediments were ultrasonically extracted three times with DCM: MeOH (9:1, v/v) for 15 min. Before extraction, known amounts of 2-nonadecanone, androstanol and C_{46} GDGT were added as internal standards. Supernatants of each extraction were obtained by centrifugation. The total lipid extracts were combined and concentrated with rotary evaporation to ~1 mL, and saponified for 2 h at 80 °C with 1 mL of KOH (0.1 M) in MeOH: H_2O (9:1, v/v). The neutral fractions were extracted with *n*-hexane, and were further separated into alkane, alkenone and alcohol sub-fractions (containing diols and GDGTs) by column chromatography on silica gel using *n*-hexane, DCM: *n*-hexane (2:1, v/v) and DCM: MeOH (1:1, v/v), respectively.

2.3 Alkenone analysis and $U^{K'}_{37}$ index

Alkenones were analysed using a 7890A gas chromatograph (GC, Agilent Technologies) equipped with a cold on-column injection system, a DB-5MS fused silica capillary column (60 m, ID 250 μm, 0.25 μm film coupled to a 5 m, ID 530 μm deactivated fused silica precolumn) and a flame ionization detector (FID). Helium was used as carrier gas (constant flow, 1.5 mL/min) and the GC oven was heated using the following temperature program: 60 °C for 1 min, 20 °C/min to 150 °C, 6 °C/min to 320 °C and a final hold time of 35 min. Di-unsaturated ($C_{37:2}$) and tri-unsaturated ($C_{37:3}$) alkenones were identified by comparison of the retention times with a reference sample composed of known compounds. Peak areas were determined by integrating the respective peaks, and concentrations were calculated using the response factor of the internal standard 2-nonadecanone.

The $U^{K'}_{37}$ index was calculated using Eq. (1) after Prahl and Wakeham (1987).

$$U^{K'}_{37} = \frac{C_{37:2}}{C_{37:2}+C_{37:3}} \quad (1)$$

SST was estimated using Eq. (2) from Conte et al., (2006) with a calibration error of 1.1 °C:

$$\text{SST } (°C) = \frac{U^{K'}_{37} - 0.0709}{0.0322} \quad (2)$$

The uncertainty of $U^{K'}_{37}$ index (0.01) was determined from a reference standard, which was co-analysed with samples for half year in our lab (n = 24). After converted to SST using Eq. (2), the analytical error for $U^{K'}_{37}$-derived SST is 0.31 °C, which is much lower than the calibration error.

2.4 Long chain diol analysis

One half of each alcohol fraction was silylated with N, O-bis(trimethylsilyl)-trifluoroacetamide (BSTFA)/1% trimethylchlorosilane (TMCS) and acetonitrile (30 µL each) and heated at 60 °C for 1 h. Diols were analysed by gas chromatography-mass spectrometry (GC/MS) on an Agilent 6850 GC coupled to an Agilent 5975C MSD operating in electron impact (EI) mode with an ionization energy of 70 eV. The GC was equipped with a fused silica capillary column (Restek Rxi-1ms, length 30 m; 250 µm ID, film thickness 0.25 µm). Helium was used as carrier gas at a constant flow rate of 1.2 mL/min. Samples (1 µL) were injected in splitless mode in a split/splitless injector (S/SL) held at 280 °C. The GC temperature program was as follows: 60 °C start temperature, held for 3 min, increased to 150 °C at a rate of 20 °C/min, increased further to 320 °C at a rate of 4 °C/min and finally held at 320 °C for 15 min. The source temperature of the MS was set to 230 °C and the quadrupole to 150 °C.

For identification of the diols, the MS was operated in single-ion monitoring (SIM) mode with the following m/z: 313.3 (C_{28} 1,13-diol, C_{30} 1,15-diol), and 341.3 (C_{30} 1,13-diol, C_{32} 1,15-diol) (Versteegh et al., 1997; Rampen et al., 2012). Fractional abundances of the long chain diols were calculated from integrated relevant peak areas in respective mass chromatograms.

The LDI was calculated and converted to SST using Eq. (3) and Eq. (4) from Rampen et al. (2012) (The calibration error of SST is 2 °C):

$$\mathrm{LDI} = \frac{[\mathrm{C_{30}\ 1,15}]}{[\mathrm{C_{28}\ 1,13}] + [\mathrm{C_{30}\ 1,13}] + [\mathrm{C_{30}\ 1,15}]} \quad (3)$$

$$\mathrm{SST\ (°C)} = \frac{\mathrm{LDI} - 0.095}{0.033} \quad (4)$$

The $\%C_{32}$ 1,15 index reflecting riverine input was calculated using Eq. (5) given by Lattaud et al. (2017) as follows:

$$\%\mathrm{C_{32}\ 1,15} = \frac{[\mathrm{C_{32}\ 1,15}]}{[\mathrm{C_{32}\ 1,15}] + [\mathrm{C_{30}\ 1,15}] + [\mathrm{C_{28}\ 1,13}] + [\mathrm{C_{30}\ 1,13}]} \times 100 \quad (5)$$

During the analysis there was no reference sample for diol measurement in our lab, so the uncertainty of LDI is unknown. To confirm the potential sources of different diols in our study area, we performed a Pearson correlation coefficient (PCC) analysis using the SPSS software according to the SPSS tutorials: Pearson correlation (https://libguides.library.kent.edu/SPSS/PearsonCorr).

2.5 GDGT analysis and indices ($\mathbf{TEX_{86}^{H}}$, BIT, MI, and RI-OH)

GDGTs were analysed by high performance liquid chromatography (HPLC) coupled via an atmospheric pressure chemical ionization (APCI) interface to a single quadrupole mass spectrometer (MS), with a method slightly modified from Hopmans et al. (2016). Analyses were performed on an Agilent 1200 series HPLC system and an Agilent 6120 MSD. Separation of the individual GDGTs including the 5-/6-methyl isomers of branched-GDGTs was achieved on two UPLC silica columns in series (Waters Acquity BEH HILIC, 2.1×150 mm, 1.7 µm), with a 2.1×5 mm pre-column of the same material maintained at

30 °C. Mobile phase A and B consisted of *n*-hexane: chloroform (99:1, v/v) and *n*-hexane: 2-propanol: chloroform (89:10:1, v/v/v), respectively. After sample injection (20 µL) and 25 min isocratic elution with 18 % mobile phase B, the proportion of B was linearly increased to 50 % within 25 min, and thereafter to 100 % for the next 30 min. After another 5 min and prior to the analysis of the next sample, the column was re-equilibrated with 18 % B for 15 min. The flow rate was 0.22 mL/min and a maximum back pressure of 220 bar was obtained. The total run time was 100 min.

GDGTs were detected using positive ion APCI-MS and selective ion monitoring (SIM) of their $(M+H)^+$ ions (Schouten et al., 2007) or abundant ion-source fragmentation products of OH-GDGTs (Liu et al., 2012). APCI spray-chamber conditions were as follows: nebulizer pressure 50 psi, vaporizer temperature 350 °C, N_2 drying gas flow 5 L/min and 350 °C, capillary voltage (ion transfer tube) −4 kV and corona current +5 µA. The MS-detector was set for SIM of the following $(M+H)^+$ ions: m/z 1302.3 (GDGT-0), 1300.3 (GDGT-1+OH-GDGT 0), 1298.3 (GDGT-2+OH-GDGT-1), 1296.3 (GDGT-3+OH-GDGT-2), 1292.3 (GDGT-4+4´/Crenarchaeol+isomer), 1050 (GDGT-IIIa/IIIa'), 1048 (GDGT-IIIb/IIIb'), 1046 (GDGT-IIIc/IIIc'), 1036 (GDGT-IIa/IIa'), 1034 (GDGT-IIb/IIb'), 1032 (GDGT-IIc/IIc'), 1022 (GDGT-Ia), 1020 (GDGT-Ib), 1018 (GDGT-Ic) and 744 (C_{46} standard), with a dwell time of 57 ms per ion.

Quantification of the individual GDGTs was achieved by integrating the respective peak areas. Compound contents were calculated using the response factor obtained from the C_{46} standard and by normalizing to the amount of extracted sediment. Due to the lack of appropriate standards, individual relative response factors between the C_{46} standard and the different GDGTs could not be considered, the obtained concentrations should therefore be regarded as being only semi-quantitative.

The TEX_{86} and TEX_{86}^H were calculated following Eq. (6) and Eq. (7) and converted to SST according to Eq. (8) given by Kim et al. (2010), which is suitable to reconstruct SST between 15 and 30 °C with a calibration error of 2.5 °C.

$$TEX_{86} = \frac{GDGT\text{-}2 + GDGT\text{-}3 + Cren'}{GDGT\text{-}1 + GDGT\text{-}2 + GDGT\text{-}3 + Cren'} \quad (6)$$

$$TEX_{86}^H = \log(TEX_{86}) \quad (7)$$

$$SST\ (°C) = 68.4 \times TEX_{86}^H + 38.6 \quad (8)$$

The uncertainty of TEX_{86}^H index (0.01) was also determined from a reference standard, which was co-analysed with samples for 3 months in our lab (n = 20). After converted to SST using Eq. (8), the analytical error for TEX_{86}^H-derived SST is 0.68 °C, which is much lower than the calibration error.

The BIT index was calculated according to Hopmans et al. (2004) including 6-methyl brGDGTs (DeJonge et al., 2013):

$$BIT = \frac{Ia + IIa + IIIa + IIa' + IIIa'}{Ia + IIa + IIIa + IIa' + IIIa' + Cren} \quad (9)$$

where Ia is the basic tetramethyl brGDGT; IIa and IIIa are 5-methyl brGDGTs; IIa' and IIIa' are 6-methyl brGDGTs (DeJonge et al., 2013).

The methane index (MI) was calculated using the Eq. (10) given by Zhang et al. (2011):

$$MI = \frac{GDGT\text{-}1 + GDGT\text{-}2 + GDGT\text{-}3}{GDGT\text{-}1 + GDGT\text{-}2 + GDGT\text{-}3 + Cren + Cren'} \quad (10)$$

The ring index (RI) was calculated using the Eq. (11) (Zhang et al., 2016)

$$RI = 0 \times [GDGT\text{-}0] + 1 \times [GDGT\text{-}1] + 2 \times [GDGT\text{-}2] + 3 \times [GDGT\text{-}3] + 4 \times [Cren] + 4 \times [Cren'] \quad (11)$$

The RI-OH index was calculated using Eq. (12), and converted to annual mean SST with the calibration error of 2 °C according to Eq. (13) (Lü et al., 2015):

$$RI\text{-}OH = \frac{[OH\text{-}GDGT\text{-}1]+2\times[OH\text{-}GDGT\text{-}2]}{[OH\text{-}GDGT\text{-}1]+[OH\text{-}GDGT\text{-}2]} \quad (12)$$

$$SST\ (°C) = \frac{RI\text{-}OH - 0.92}{0.028} \quad (13)$$

The uncertainty of RI-OH index (0.01) was also determined from a reference standard, which was co-analysed with samples for 3 months in our lab (n = 20). After converted to SST using Eq. (13), the analytical error for RI-OH-derived SST is 0.36 °C, which is much lower than the calibration error.

2.6 Climatological mean temperature data and temperature residuals of proxies

Annual and seasonal SST data (Table 1) for each sampling site were 13-years average values (2005–2017) taken from the NOAA World Ocean Atlas 2018 (WOA18) on a 0.25° grid resolution (https://www.nodc.noaa.gov/cgi-bin/OC5/woa18/woa18.pl), which is the latest version and close to the estimated deposition time ([sampling time, 2012–2017)] – [depth, 0–2 cm)]/[deposition rate, 2-6 mm yr^{-1}] = [deposition time, 2002-2014)) (Ge et al., 2014; Liu et al., 2014). According to the description of WOA18, seasons were defined as follows: Winter: January–March; Spring: April–June; Summer: July–September; Autumn: October–December.

In our study region, spatial SSTs in each season varied in a small range, with the largest in winter but still <6 °C. Together with influences of factors other than SST on proxies, this usually leads to poor SST-proxy correlations for all seasons, albeit likely slightly better for winter data. So we did not use correlation as a criterion to decide seasonality. Instead, we used another common criterion, i.e., temperature residuals between calculated temperatures from established calibrations and WOA18-derived seasonal SSTs, calculated as below:

$$Residual\ (°C) = [proxy\text{-}derived\ temperature] - [WOA18\text{-}derived\ temperature] \quad (14)$$

3 Results

3.1 Hydrological parameters

Except one sample taken from deeper waters (LD-21, WD = 1307 m), the sites of surface sediment samples in this study were mainly located on the shelf area (WD <200 m) (Fig. 1a). The measured annual mean SSTs (0 m depth, from the

WOA18 dataset) in the study area ranged between 24.2 °C and 27.0 °C (25.6 °C average), and showed clear seasonal variations exhibiting low values in winter (21.6 °C average), highest in summer (29.0 °C average), and intermediate in spring (26.2 °C average) and autumn (25.6 °C average) (Fig. 2 and Table 1). Note that spring, autumn and annual temperatures are very close to each other. The temperatures of the mixed layer (0–30 m) were slightly (<0.7 °C) lower than SST and also varied seasonally in a similar pattern (Suppl. Table 1). The annual mean and seasonal SSTs displayed an increasing trend offshore with the largest difference of ca. 6 °C in winter between inshore and offshore (Fig. 2).

3.2 $U^{K'}_{37}$ and alkenone-derived temperatures

The $U^{K'}_{37}$ index ranged between 0.81 and 0.94 (0.91 average, Table 1), corresponding to 23.0–27.0 °C (26.0 °C average, Fig. 2a) based on the linear calibration proposed by Conte et al. (2006). Compared with the measured SSTs, the $U^{K'}_{37}$-SSTs were closest to the spring or annual mean SSTs at most sites, except the two inshore samples (WD <50 m) showing slightly lower $U^{K'}_{37}$-SSTs (Fig. 2a). Since $U^{K'}_{37}$-Temperature relationship has been found to be non-linear at SSTs >24–26°C (e.g., Conte et al., 2006, Sonzogni et al., 1997, Tierney and Tingley, 2018), we also compared results from different calibrations, including linear and non-linear calibrations for 0 m or 0–30 m SSTs (Fig. 3), and found that all derived $U^{K'}_{37}$-SSTs exhibited similar values within 0.5 °C (0.2 °C average; Suppl. Table 2). Specially, the recently proposed Bayesian B-spline regression model, BAYSPLINE (Tierney and Tingley, 2018), yielded higher values by 0.5 °C than those from the linear calibration of Conte et al. (2006).

3.3 LCD distribution and LDI-derived temperatures

In the total 1,13- and 1,15-diols, the C_{30} 1,15-diol was the most abundant (>80 %) at most sites outside the PRE, followed by C_{32} 1,15-diols (<15 %) and C_{28} and C_{30} 1,13-diols (<4 %) (Fig. 4a–4d). However, the C_{32} 1,15-diols were more abundant (>41 %) than the C_{30} 1,15-diols (>19 %) in the PRE sediments (Fig. 4c and 4d). The C_{28} and C_{30} 1,13-diols exhibited a similar spatial distribution pattern as the C_{32} 1,15-diol, showing higher relative abundances in the PRE and coastal area (Fig. 4a, 4b and 4d). PCC analysis also showed C_{28} and C_{30} 1,13-diols and C_{32} 1,15-diols were significantly correlated between each other (correlation coefficient: 0.56–0.83, p <0.005, Table 2). In contrast, these three diols were negatively correlated with C_{30} 1,15-diol (correlation coefficient from −0.68 to −0.90, p <0.005, Table 2), with the latter exhibiting an opposite pattern and showing an overall increasing trend towards the offshore.

The LDI values of surface sediments varied from 0.56 to 0.98 (Table 1), but were ≥0.90 at most sites, corresponding to LDI-derived temperatures (LDI-SST) varying from 14.0 to 26.9 °C (Fig. 2b). The river input index (%C_{32} 1,15) values ranged from 1.9 % to 66.3 %, showing an overall decreasing trend offshore (Fig. 4d and Suppl. Table 3).

3.4 Distribution of iGDGTs and TEX_{86}^{H}-derived temperatures

The iGDGTs were dominated by crenarchaeol ([Cren], 43.2–65.9 %) and GDGT-0 ([0], 18.1–37.0 %) (Fig. 5a–5f), and the ratios of both compounds, i.e. [0]/[Cren], ranged between 0.28 and 0.75 (Fig. 5h). Two samples with relatively high values of [0]/[Cren] were from the PRE (0.75, PRE-A8) and the deep sea (0.69, LD-21) (Fig. 5h). The least abundant iGDGTs is the crenarchaeol isomer ([Cren'], 0.8–5.4 %), showing an overall increasing trend offshore (Fig. 5f). The ratio of GDGT-0 and crenarchaeol isomer, i.e. [0]/[Cren'], maximized in the river mouth (47.3, PRE-A8) and exhibited a declining trend offshore (Fig. 5i). The ratio of GDGT-2 versus GDGT-3, i.e. [2]/[3], ranged from 2.6 to 7.2, and was low at shelf and coastal sites (WD <200 m, 2.6–3.6), but high at the deep-sea site (7.2, LD-21) (Fig. 5i). Similar spatial distribution patterns appeared also for the [2]/[Cren] ratio and the MI value, exhibiting low values of 0.07–0.15 for [2]/[Cren] and 0.16–0.26 for MI at shelf and coastal sites, and slightly higher values of 0.25 for [2]/[Cren] and 0.31 for MI at the deep-sea site (LD-21) (Fig. 5g). In addition, higher BIT values (0.49) were found in the PRE, relative to the inshore area (0.1–0.3, WD <50 m) and the offshore area (<0.1) (Fig. 5h).

TEX_{86}^{H} values varied in the range between −0.33 and −0.18 (Table 1), corresponding to SST values of 16.2 to 26.0 °C based on the global calibration by Kim et al. (2010) (Fig. 2c and Suppl. Table 4). The annual residuals ranged from −8.8 to −1.0 °C. Seasonally, the mean absolute values of residuals were 2.0 °C, 5.9 °C, 8.6 °C and 5.3 °C, respectively, from winter to autumn (Suppl. Table 4), indicating TEX_{86}^{H}-SSTs were closer to winter temperature. Spatially, consistently low temperature estimates were found in the coastal area and PRE with water depth <50 m, some of them even colder than winter SST (Fig. 2c). However, the offshore samples had relatively high TEX_{86}^{H}-SSTs, which were ca. 2 °C higher than winter SST and close to autumn and annual SSTs (Fig. 2c). We also applied the recently proposed BAYSPAR (Bayesian SPAtially-varying Regression) calibration to our data, which yielded similar results but slightly reduced residuals (Fig. 6b and Suppl. Table 4).

3.5 Distribution of OH-GDGTs and RI-OH-derived temperatures

The OH-GDGTs contributed 1.5–4.1% to the total GDGT pool (Suppl. Table 5), consistent with the lower relative OH-GDGTs abundance found in (sub)tropical regions (Huguet et al., 2013). The most abundant OH-GDGT is OH-GDGT-2 ([OH-2], 39.2–67.0 %), with high values at shelf and coastal sites (WD ≤186 m) (Fig. 5l), but low contribution at the deep-sea site (LD-21). In contrast, the relative abundance of OH-GDGT-0 ([OH-0]) remained low at shelf and coastal sites, but was elevated at the deep-sea site (Fig. 5j).

The RI-OH values varied from 1.57 to 1.79 (Table 1), which agrees with recently reported data for the same region (1.50–1.75) (Lü et al., 2015; Yang et al., 2018). SST estimates based on the calibration suggested by Lü et al. (2015) for the Chinese marginal sea (CMS), were within a range of 23.3–31.2 °C (Fig. 2d and Suppl. Table 5). In comparison with the measured annual SST, three higher RI-OH-SSTs occurred in the PRE, with annual residuals of 2.4–6.0 °C, and other samples exhibited slightly higher or lower RI-OH-SSTs, with annual residuals of −2.4–2.9 °C (Suppl. Table 5).

4 Discussion

4.1 Seasonality of the $U_{37}^{K'}$ proxy

Although the relationship between $U_{37}^{K'}$ and SST is robust and well supported by culture studies (Conte et al., 1998; Prahl and Wakeham, 1987; Prahl et al., 1988; Sawada et al., 1996; Volkman et al., 1995), the seasonality of production of alkenones and the response of $U_{37}^{K'}$ to temperature at very warm and cold environments remain unresolved (Tierney and Tingley, 2018). Sediment trap studies demonstrated that alkenone production varies markedly across the oceans (e.g., Rosell-Melé and Prahl, 2013 and references therein), with factors such as temperature, nutrients, light availability, and competition regulating the timing of haptophyte blooms (Rosell-Melé and Prahl, 2013). The seasonality of alkenone production may be transferred to sediments, but this signal could also be altered by the complex sedimentation processes, e.g., lateral advection and resuspension (Rosell-Melé and Prahl, 2013).

Our results indicate that the linear calibration-derived $U_{37}^{K'}$-SST reflect approximately the annual mean SST but slightly spring biased in this region (Fig. 2a and 3a). And if BAYSPLINE-derived $U_{37}^{K'}$-SST is considered, the spring bias is more apparent (Fig. 3a). But the small temperature difference between the annual mean and spring SSTs precludes a clear discrimination between them. However, an inshore-offshore transect study by Zhang et al. (2013) proposed $U_{37}^{K'}$-SST to be spring- and summer-biased in this region. We note that the summer in that work included June, July and August, differing from the definition used here that the month of June is included in spring. So we are disposed to believe that the alkenone production is biased to warm season, when alkenone-sourced organisms likely develop. This proposition is consistent with the observations that coccolithophores, especially the alkenone producer *E. huxleyi*, are lowest during winter but abundant during warm months on the SCS shelf (Chen et al., 2007). During cool months, diatoms outcompete other phytoplankton due to replete surface nutrient on the shelf (Chen et al., 2007). This scenario is in contrast to the oligotrophic basin of the SCS, where elevated nutrients, still insufficient to support diatom dominancy, lead to highest coccolithophore abundance during cool months due to strong winter wind-induced mixing (Chen et al., 2007). Besides, we surmise that the warm season development of coccolithophores could also be associated with the Pearl River input, which is highest in late spring (May to June) in an annual cycle with high nutrient levels characterized by N:P ratios as high as ~100:1 (Dai et al., 2008; Lu and Gan, 2015; Xu et al., 2008; Zhang et al., 2013). Such an unbalanced nutrient ratio could stimulate the growth of alkenone-producing haptophytes, e.g., *E. huxleyi*, during this period, since both in situ investigations and experiments have reported that *E. huxleyi* have a competitive advantage over other phytoplankton at high N:P ratios (Riegman et al., 1992, Tyrrell and Taylor, 1996). This phenomenon is likely because the species has a greater activity of the enzyme alkaline phosphatase, facilitating its assimilation of dissolved organic phosphates (Bijma et al., 2001). Nevertheless, the ecology of coccolithophores on the shallow SCS shelf has not been extensively studied and future works are needed to combine phytoplankton, nutrients, water column structure and salinity investigations.

4.2 LCDs and LDI-derived temperatures

4.2.1 Source of LCDs in the surface sediments

The unusually low LDI-derived SST estimates relative to the measured SSTs observed near the coast and close to the river mouth (Fig. 2a and 4e) suggest that LDI may be influenced by terrestrial/freshwater sources other than marine producers. Similar findings were reported from the Iberian margin (de Bar et al., 2016), in the Gulf of Lion, the Berau Delta, the Kara Sea (Lattaud et al., 2017) and the East China Sea (He et al., 2020), suggestive of terrestrial influence on LCD compositions. Culture studies show that marine eustigmatophyte algae mainly produce 1,13 and 1,15-diols (Rampen et al., 2007, 2014a; Volkman et al., 1999). In freshwater environments, eustigmatophyte algae primarily produce C_{32} 1,15-diol, especially in stagnant waters during dry seasons, when rivers have low-stands (Häggi et al., 2019; Lattaud et al., 2017; Rampen et al., 2014b). However, C_{30} 1,15-diols are generally found to be dominant both in the marine water column and sediments and are likely produced by marine eustigmatophyte algae (Balzano et al., 2018).

In this study, the co-occurrence of high abundance of C_{28} and C_{30} 1,13-diols and C_{32} 1,15-diols in the PRE and along the coast rather than in the offshore area (Fig. 4a, 4b, 4d) is consistent with the PCC analysis, and further suggests a terrestrial/freshwater source of them. Such a spatial distribution pattern becomes more apparent when diol compositions in SPM and sediments are illustrated from the PRE to the offshore (Fig. 4g). In contrast, the negative correlation of C_{30} 1,15-diol with three other diols could be attributed to their different sources, i.e. marine vs. terrestrial.

4.2.2 Influence of riverine LCDs

It has been pointed out that LCDs delivered by rivers can substantially affect LDI temperature estimates in coastal regions close to river mouths (e.g., Lattaud et al., 2017; He et al., 2020). Lattaud et al. (2017) pointed out that $\%C_{32}$ 1,15 in the typical marine sediments generally does not exceed a value of 20%, which may be used as a cut-off for the reliable reconstruction of LDI-SST, and $\%C_{32}$ 1,15 >20 % implies an increased contribution of riverine LCDs. In our samples, the LDI-SST was similar to the measured annual SST at most sites (Fig. 2b), with 6 exceptions at shallow sites (<26 m) in the PRE and the near-coastal area showing temperature values underestimated by as great as −11.0 °C (Fig. 2b and 4e). We found the greater underestimations corresponded to $\%C_{32}$ 1,15 values that are >20 % and 4× higher than those of the other samples and the samples with $\%C_{32}$ 1,15 <20 % have smaller annual residuals ranging between −0.2 °C and 1.2 °C (Fig. 4e and Suppl. Table 3). Besides, the $\%C_{32}$ 1,15 values correlated positively (R^2 = 0.66, p <0.001) with the BIT index that is often used to indicate terrestrial input in the coastal area (Fig. 4f). So $\%C_{32}$ 1,15 is also effective to indicate river input in this region. After removal of data points (n = 6) with $\%C_{32}$ 1,15 >20%, indicating significant influence of riverine LCDs, the LDI-SST of the reduced data set yield a mean value of absolute annual SST residuals of 0.5 °C, nearly half of those of the full data set.

4.2.3 Seasonality of LDI index

Our results indicated that LDI-SSTs with minimal river influences may reflect annual SSTs (Fig. 2b and Suppl. Table 3), suggesting unbiased seasonal production of the source organisms of LDI in this study area. Similar results have been reported by Zhu et al. (2014), who found that LDI-SSTs in downcore sediments matched well with local annual SSTs in the northern SCS. Rampen et al. (2007) found comparable annual flux of 1, 15-diols at different stations in the Arabian Sea, and suggested that the biological producers of 1,15-diols do not require a high level of nutrients as needed by, e.g., *Proboscia* diatoms. Thus, LDI may reflect annual SST due to a lack of sensitivity of marine eustigmatophytes to nutrient variations in an annual cycle in the northern SCS shelf.

4.3 TEX_{86}^{H} and isoprenoid GDGT-derived temperature estimates

4.3.1 Sources of iGDGTs in the surface sediments

In marine sediments, the iGDGTs composition may sometimes be impacted with or even controlled by non-thermal factors, e.g., sources of iGDGTs other than Thaumarchaeota (Zhang et al., 2016). Several indices, e.g., the MI, BIT, and the [2]/[Cren] ratio have been developed to assess these impacts. Relatively low MI values (≤0.25) were observed at most sites here accompanied by low [2]/[Cren] ratios (0.07–0.15) (Fig. 5g). These values may suggest little input of iGDGTs from archaea involved in methane cycling that are typically characterized by a high MI value (>0.3) or substantially elevated [2]/[Cren] ratio (>0.2) (Weijers et al., 2011; Zhang et al., 2016). The exception was the deep-sea sample (LD-21), showing a slightly higher MI value (0.31) and a higher [2]/[Cren] ratio of 0.25, which could be slightly associated with the archaea involved in methane cycling. The constantly low BIT values at most sites are typical for marine sediments with little terrestrial impact. The highest BIT value (0.49) observed in the PRE (sample PRE-A8) (Fig. 5g) is similar to the finding of Zhang et al. (2012). As the BIT index in soils generally tends to be >0.9 (Hopmans et al., 2004), the highest BIT value at the site likely indicates a significant input of soil-derived GDGTs. However, the ability of the BIT index to indicate soil input in this region has recently been discounted by the finding that branched GDGTs may be aquatically in-situ produced (Zhou et al., 2014). Nevertheless, considering that the sample PRE-A8 is located at the upper river mouth, together with the highest $\%C_{32}$ 1,15 values as discussed above, we believe iGDGTs may be impacted to some extent by terrestrial input.

The [0]/[Cren] ratio was also high at the site PRE-A8. This is likely associated with river input, as the [0]/[Cren] ratio has been found to be high (>2) in soils and river sediments likely due to in situ methanogenic archaea or imported soil-derived methanogens (Wang et al., 2015; Zhu et al., 2011). Slightly different from other iGDGTs, [Cren'] increased clearly with increasing water depth, with the lowest value of 0.8 % found in the PRE (PRE-A8) and ~1.0 % close to the PRE (Fig. 5f). This pattern was unlikely caused by soil iGDGTs input, as [Cren'] in the soils in the catchments of the Pearl River is ~3 % (Wang et al., 2015). Recently, [Cren'] as low as 0.2–0.7 %, with a mean of 0.4 %, was observed in the SPM of the lower Pearl River, which was attributed to the predominance of Euryarchaeota (Wang et al., 2015; Xie et al., 2014). In contrast,

[Cren'] in deep-sea sediments in the SCS is also characterized by higher values >4 % (Jia et al., 2017). So, iGDGTs close to and within the PRE could also be impacted by in situ archaea input other than Thaumarchaeota.

Recently, several studies suggest that tetraether lipids of Thaumarchaeota dwelling in shallow waters are characterized by [2]/[3] ratios <4 and [Cren'] <4 %, whereas for "deep-water" Thaumarchaeota lipids are characterized by higher values (Jia et al., 2017; Kim et al., 2015, 2016). The difference in iGDGTs distributions between the two eco-types of Thaumarchaeota is due likely to the use of different enzymes for iGDGTs synthesis (Kim et al., 2016; Villanueva et al., 2015). Based on these criteria, only one sample, i.e. the deep-sea sample LD-21 with a [2]/[3] ratio of 7.2 and [Cren'] of 5.4 % (Fig. 5f, 5i), likely received some contributions from deep Thaumarchaeota. The sample at the second deepest site, i.e. E503 at 186 m, showed a [2]/[3] ratio of 3.6 and [Cren'] of 4.3 % (Fig. 5f, 5i), which suggests only a small contribution from deep Thaumarchaeota. The occurrence of low [2]/[3] ratios and low [Cren'] fractional abundances for most of our study sites is in agreement with the shallow water depths of these sites, as the depth boundary to separate the deep and shallow Thaumarchaeota, although not exactly determined, is likely 200–300 m (Jia et al., 2017; Kim et al., 2015, 2016).

Recently, Zhang et al. (2016) proposed that the relation between TEX_{86} and Ring Index (RI) can be used to assess if the TEX_{86} is influenced by non-thermal factors. Unexpectedly, using the global TEX_{86}-RI relationship (Zhang et al., 2016), we found most of our sediment data lay out of the 95% prediction band (Fig. 6a), likely negating TEX_{86} of our sample to indicate seawater temperature. However, except the two samples (LD-21 and PRE-A8) that may be influenced by other factors as discussed above, our data lay within the 95 % prediction of "shallow-water" TEX_{86}-RI relationship (Fig. 6a) derived from the surface water SPM (Jia et al., 2017). We think the latter is reasonable because: (1) our study sites receive predominantly shallow Thaumarchaeota input as demonstrated above, and (2) the shallow Thaumarchaeota likely respond to ambient temperature differently from the deep ones (Jia et al., 2017; Kim et al., 2015, 2016; Taylor et al., 2013; Villanueva et al., 2015), hence causing a different shallow-water TEX_{86}-RI relationship from the global that contains mainly deep-sea sedimentary data. Therefore, TEX_{86} in most of our sediments may still indicate seawater temperature changes.

Besides, in a recent study in the East China Sea shelf, Zhang et al. (2017) noted the impact of the resuspension and lateral transport on the TEX_{86} proxy, which could not break the TEX_{86}-RI relationship but may make the TEX_{86}-SST relationship irregular. In our results, some large scatters of TEX_{86}^{H}-derived SSTs from the measured SSTs (Fig. 2c) perhaps were partly associated with the resuspension and lateral transport. However, as shown below the scatters are more likely caused by the calibration.

4.3.2 Seasonality of TEX_{86}^{H} index

Based on the above discussion on iGDGTs indices, only two samples, one in the PRE (PRE-A8) and the other in the deep sea (LD-21), are markedly different from the remaining samples that appear minimally influenced by soil/freshwater-derived archaea and deep-dwelling Thaumarchaeota or methane-cycling archaea. After excluding these two samples, we examined the temperature signal of the TEX_{86}^{H} index as below.

In the coastal area of northern SCS, TEX_{86}^{H}-derived SST in surface sediments and surface water SPM has been found lower than annual SST and hence attributed to winter-biased archaeal production and associated iGDGTs burial (Ge et al., 2013; Wei et al., 2011; Zhang et al., 2012; Zhou et al., 2014). Our TEX_{86}^{H}-SST estimates were 0.9–8.8 °C lower than annual SST, similar to previous studies. However, when compared with winter SST, the residuals varied between −4.7 and 2.1 °C, still showing some large negative residuals (Fig.6b and Suppl. Table 4). The BAYSPAR estimates yielded similar results to TEX_{86}^{H}-SST estimates, although the residuals were slightly reduced by ~0.3 °C (Fig. 6b and Suppl. Table 4).

We noted that different from the global dataset utilized to establish the TEX_{86}^{H}-SST (i.e. Eq. (8)), which includes a large number of deep-sea sediment samples, our data here were exclusively from shallow sediments receiving iGDGTs predominantly from shallow dwelling Thaumarchaeota. Therefore, we surmise that the global TEX_{86}^{H}-SST calibration might not be accurate for our study area, due to that the shallow and deep Thaumarchaeota exhibit slightly different tetraether compositions. Alternatively, a local "shallow-water" calibration could be more appropriate for temperature reconstruction in this study. So a recent seasonal calibration based on winter surface water SPM in the SCS (Jia et al., 2017) was applied to our data as a comparison. By applying the equation established from winter SPM ($SST_{winter} = 47.18 \times TEX_{86}^{H} + 34.44$, n = 45, $R^2 = 0.6$; Jia et al., 2017), we found that the winter residuals were greatly reduced, ranging between –2.1 to 2.0 °C (Fig. 6b), with only two samples having residuals greater than 2 °C. This suggests that iGDGTs-derived temperature is really winter biased in the SCS shelf, and the local calibration is powerful for temperature reconstruction.

4.4 RI-OH and RI-OH-derived temperatures

4.4.1 Source of OH-GDGTs and their influences on RI-OH-SST estimates

A few studies have detected OH-GDGTs in marine, river, lacustrine and soil environments, indicating ubiquitous and multiple sources of OH-GDGTs (Chen et al., 2016; Huguet et al., 2013; Kang et al., 2017; Liu et al., 2012; Park et al., 2019; Wang et al., 2012). Kang et al. (2017) noted that OH-0 (OH-GDGT-0) dominated in marine and estuarine environments (56 ± 10 %), but OH-2 (OH-GDGT-2) was abundant in lake, river and soil environments, which may lead to overestimated RI-OH-SSTs in case of substantial terrestrial input. Consistently, our results showed that RI-OH-SSTs were warm-biased in the PRE (Fig. 2d), where terrestrial input is significant.

In the SCS, there have been some sedimentary OH-GDGTs data reported previously from water depths ranging between 3 m and 4405 m (Lü et al., 2015; Yang et al., 2018). By combining our data with those published SCS data, there was a very significant positive logarithmic correlation between [OH-0] and water depth ($R^2 = 0.66$, $p < 0.001$, Fig. 5j), but a very significant negative logarithmic correlation between [OH-2] and water depth ($R^2 = 0.53$, $p < 0.001$, Fig. 5l). We also found that, with the exception of one sample (WD = 41 m), two clusters of samples can be separated based on the [OH-0]/[OH-2] ratio, with the ratio value <0.55 for the shallow-water samples (WD ≤186 m, including all data in this study) and >0.55 for the deep-water samples (WD ≥330 m) (Fig. 7a). This is abnormal because the deep-water samples were located in slope and basin of the SCS at the lower latitudes with higher SSTs (Yang et al., 2018), which should induce more abundance of OH-2

according to eq. (12). For the shallow-water samples the annual residuals were bassically not affected by SST, whereas for the deep-water samples they became increasingly negative with the increase of SST from ca. 26–29 °C (Fig. 7b). This phenominon is quite similar to the recent finding that the fractional abundance of OH-2 is negatively related with SST when SST is >25 °C (Yang et al., 2018), although data from a modified Bligh/Dyer method was analyzed in that work. Nevertheless, the data from the same ultrasonic extraction method showing that the shallow-water samples exhibited annual RI-OH-SST residuals of −2.5 °C to 3.4 °C, but the deep-water samples showed a larger and more negative range between −8.1 °C and 2.3 °C (Fig. 7b, c), likely implying a winter or deeper bias of the RI-OH in deep sea sediments. Considering the less degree of seasonality of the tropical SCS basin and the siginificant negative correlation of SST with the water depth (R^2 = 0.74, p <0.001, Fig. 7c), we postulate that archaea dwelling in the cool/cold deep water or sediments with lower abundance of OH-2 could have contributed to the deep-water sedimentary OH-GDGTs. This interpretation is different form Yang et al. (2018), who propose OH-2 abundance may respond to temperature inversely at higher SSTs (>25 °C). In fact, all of our samples belonged to the shallow-water samples, and their RI-OH (or [OH-2]) was positively correlated with annual SST although the annual SSTs of most data (n = 13 of 16) were above 25 °C (Fig. 7d). As a comparison, most samples of Yang et al. (2018) (n = 17 of 23) were located in the deep ocean (WD> 971 m) and SST generally increase coincidently with water depth (Fig. 7c).

4.4.2 Seasonality of RI-OH-temperature relation in surface sediments

In the China coastal seas (CCSs), in addition to the good relation between RI-OH and annual SSTs (R^2 = 0.81, p <0.01), Lü et al. (2015) also found that the RI-OH index is significantly correlated with seasonal SSTs with all R^2 >0.77, and hence proving a calibrations for each season. We applied these four seasonal calibrations to our RI-OH data and compared them with observed seasonal SSTs from WOA18 and found that the average absolute residuals for winter, spring, summer and autumn are 1.5 (−2.4–3.6 °C), 2.3 (−5.4–3.7 °C), 0.8 (−1.3–1.4 °) and 1.9 °C (0.4–3.6 °C), respectively (Suppl. Table 5). Comparatively, the annual residuals ranged between −2.4 and 2.9 °C and averaged 1.2 °C. Thereby, the summer residuals are the lowest, suggesting that RI-OH may better represent summer SST in the SCS shelf. This occurrence is similar to the observations by Lü et al. (2015, 2019). However, TEX_{86}^{H}-derived SST is biased to winter SST in this region as discussed above, this mismatch may suggest different sources of OH-GDGTs and iGDGTs. However, the source of OH-GDGTs has not been fully clear yet, and thus more studies on OH-GDGTs in various regions are needed for a better assessment of the proxy.

5 Conclusions

Temperature estimates from $U_{37}^{K'}$, LDI, TEX_{86}^{H} and RI-OH proxies in surface sediments from the northern South China Sea shelf, including the Pearl River Estuary and the coastal area, were compared with annual and seasonal satellite-derived SSTs (WOA18). $U_{37}^{K'}$-SST was mainly spring-biased, likely due to the blooming of alkenone source-organisms in late spring, when

river runoff, as well as the abundant terrestrial nutrients, are highest. The results also showed that terrestrial inputs have an appreciable impact on LDI, TEX_{86}^{H} and RI-OH proxies and lead to cold-biased (LDI and TEX_{86}^{H}) or warm-biased (RI-OH) temperature relative to SSTs. After excluding from the data set the samples subject to terrestrial input, these indices exhibited different seasonal variabilities, which reflect distinctive ecologies of their source organisms as results of seasonal changes in environmental conditions. LDI-SST matched well with annual SSTs, possibly related with the insensitivity of marine eustigmatophytes to nutrient variations in an annual cycle. For the TEX_{86}^{H} proxy, a local "shallow-water" calibration based on winter surface water SPM in the SCS appeared more appropriate for temperature reconstruction and greatly reduced winter residuals. The winter biased TEX_{86}^{H} can likely be attributed to favorable conditions for planktonic archaea in winter, impacted by the enhancement of local vertical seawater mixing. In contrast to the TEX_{86}^{H} indices, RI-OH seems to reflect summer SST, hence suggesting different source organisms of OH-GDGTs and iGDGTs that needs further investigations.

Acknowledgements

This work is supported by the National Natural Science Foundation of China (grant No. 41676030). BW thanks the China Scholarship Council (201706260033) for the support during his stay at Alfred Wegener Institute (Germany). We acknowledge the captain, crew and scientists who participated in the expeditions for collecting samples used in this study. We appreciate the assistance from Jens Hefter for biomarker analysis at Alfred Wegener Institute. Two anonymous reviewers are grateful for their constructive comments.

Data availability

The data produced in this publication will be available from the PANGAEA database: https://doi.pangaea.de/10.1594/PANGAEA.905187.

Author contribution

GJ and GM conceived and designed the study. BW and MK collected the samples. BW conducted all the proxy analysis and was aided by JH in the instrument maintenance and data analysis. BW wrote the paper with inputs from GJ, GM and EP. All the authors reviewed the final manuscript.

Supplement

There is supplement related to this article.

References

Balzano, S., Lattaud, J., Villanueva, L., Rampen, S., Brussaard, C. P. D., van Bleijswijk, J., Bale, N., Sinninghe Damsté, J. S. and Schouten, S.: A quest for the biological sources of the ubiquitous long chain alkyl diols in the western tropical North Atlantic Ocean, Biogeosciences, 5951–5968, doi:10.5194/bg-2018-97, 2018.

de Bar, M. W., Dorhout, D. J. C., Hopmans, E. C., Rampen, S. W., Sinninghe Damsté, J. S. and Schouten, S.: Constraints on the application of long chain diol proxies in the Iberian Atlantic margin, Org. Geochem., 101, 184–195, doi:10.1016/j.orggeochem.2016.09.005, 2016.

Benthien, A. and Müller, P. J.: Anomalously low alkenone temperatures caused by lateral particle and sediment transport in the Malvinas Current region, western Argentine Basin, Deep Sea Res. Part I Oceanogr. Res. Pap., 47(12), 2369–2393, 2000.

Bijma, J., Altabet, M., Conte, M., Kinkel, H., Versteegh, G. J. M., Volkman, J. K., Wakeham, S. G. and Weaver, P. P.: Primary signal: Ecological and environmental factors-Report from Working Group 2, Geochemistry, Geophysics. Geosystems, 2(1), doi:10.1029/2000gc-000051, 2001.

Brassell, S. C., Eglinton, G., Marlowe, T., Phaumann, U.: Molecular stratigraphy: a new tool for climatic assessment, Nature, 320(6058): 129, 1986.

Chen, J., Hu, P., Li, X., Yang, Y., Song, J., Li, X., Yuan, H., Li, N. and Lü, X.: Impact of water depth on the distribution of iGDGTs in the surface sediments from the northern South China Sea: applicability of TEX_{86} in marginal seas, Front. Earth Sci., 12(1), 95–107, doi:10.1007/s11707-016-0620-1, 2018.

Chen, Y., Zhang, C., Jia, C., Zheng, F. and Zhu, C.: Tracking the signals of living archaea: A multiple reaction monitoring (MRM) method for detection of trace amounts of intact polar lipids from the natural environment, Org. Geochem., 97, 1–4, doi:10.1016/j.orggeochem.2016.04.006, 2016.

Chen, Y. ling L., Chen, H. Y. and Chung, C. W.: Seasonal variability of coccolithophore abundance and assemblage in the northern South China Sea, Deep. Res. Part II Top. Stud. Oceanogr., 54(14–15), 1617–1633, doi:10.1016/j.dsr2.2007.05.005, 2007.

Conte, M. H., Sicre, M., Rühlemann, C., Weber, J. C., Schulte, S., Schulz-Bull, D. and Blanz, T.: Global temperature calibration of the alkenone unsaturation index ($U^{K'}_{37}$) in surface waters and comparison with surface sediments, Geochemistry, Geophys. Geosystems, 7(2), doi:10.1029/2005GC001054, 2006.

Conte, M. H., Thompson, A., Lesley, D. and Harris, R. P.: Genetic and physiological influences on the alkenone/alkenoate versus growth temperature relationship in Emiliania huxleyi and Gephyrocapsa oceanica, Geochim. Cosmochim. Acta, 62(1), 51–68, doi:10.1016/S0016-7037(97)00327-X, 1998.

Dai, S. B., Yang, S. L. and Cai, A. M.: Impacts of dams on the sediment flux of the Pearl River, southern China, Catena, 76(1), 36–43, doi:10.1016/j.catena.2008.08.004, 2008.

Eglinton, T. I. and Eglinton, G.: Molecular proxies for paleoclimatology, Earth Planet. Sci. Lett., 275(1–2), 1–16,

doi:10.1016/j.epsl.2008.07.012, 2008.

Elling, F. J., Könneke, M., Lipp, J. S., Becker, K. W., Gagen, E. J. and Hinrichs, K. U.: Effects of growth phase on the membrane lipid composition of the thaumarchaeon *Nitrosopumilus maritimus* and their implications for archaeal lipid distributions in the marine environment, Geochim. Cosmochim. Acta, 141, 579–597, doi:10.1016/j.gca.2014.07.005, 2014.

Elling, F. J., Könneke, M., Mußmann, M., Greve, A. and Hinrichs, K. U.: Influence of temperature, pH, and salinity on membrane lipid composition and TEX86 of marine planktonic thaumarchaeal isolates, Geochim. Cosmochim. Acta, 171, 238–255, doi:10.1016/j.gca.2015.09.004, 2015.

Elling, F. J., Könneke, M., Nicol, G. W., Stieglmeier, M., Bayer, B., Spieck, E., de la Torre, J. R., Becker, K. W., Thomm, M., Prosser, J. I., Herndl, G. J., Schleper, C. and Hinrichs, K. U.: Chemotaxonomic characterisation of the thaumarchaeal lipidome, Environ. Microbiol., 19(7), 2681–2700, doi:10.1111/1462-2920.13759, 2017.

Farrimond, P., Eglinton, G. and Brassell, S. C.: Alkenones in Cretaceous black shales, Blake-Bahama Basin, western North Atlantic, Org. Geochem., 10(4–6), 897–903, doi:10.1016/S0146-6380(86)80027-4, 1986.

Ge, H., Zhang, C. L., Dang, H., Zhu, C. and Jia, G.: Distribution of tetraether lipids in surface sediments of the northern South China Sea: Implications for TEX_{86} proxies, Geosci. Front., 4(2), 223–229, doi:10.1016/j.gsf.2012.1G0.002, 2013.

Ge, Q., Liu, J. P., Xue, Z. and Chu, F.: Dispersal of the Zhujiang River (Pearl River) derived sediment in the Holocene, Acta Oceanol. Sin., 33(8), 1–9, doi:10.1007/s13131-014-0407-8, 2014b.

Goni, M. A., Hartz, D. M., Thunell, R. C. and Tappa, E.: Oceanographic considerations for the application of the alkenone-based paleotemperature U37K′ index in the Gulf of California, Geochim. Cosmochim. Acta, 65(4), 545–557, 2001.

Häggi, C., Schefuß, E., Sawakuchi, A. O., Chiessi, C. M., Mulitza, S., Bertassoli Jr, D. J., Hefter, J., Zabel, M., Baker, P. A. and Schouten, S.: Modern and late Pleistocene particulate organic carbon transport by the Amazon River: Insights from long-chain alkyl diols, Geochim. Cosmochim. Acta, doi:10.1016/j.gca.2019.07.018, 2019.

He, L., Kang, M., Zhang, D. and Jia, G.: Evaluation of environmental proxies based on long chain alkyl diols, Org. Geochem., 139, 103948, doi:10.1016/j.orggeochem.2019.103948, 2019.

Hopmans, E. C., Weijers, J. W. H., Schefuß, E., Herfort, L., Sinninghe Damsté, J. S. and Schouten, S.: A novel proxy for terrestrial organic matter in sediments based on branched and isoprenoid tetraether lipids, Earth Planet. Sci. Lett., 224(1–2), 107–116, doi:10.1016/j.epsl.2004.05.012, 2004.

Huguet, C., Fietz, S. and Rosell-Melé, A.: Global distribution patterns of hydroxy glycerol dialkyl glycerol tetraethers, Org. Geochem., 57, 107–118, doi:10.1016/j.orggeochem.2013.01.010, 2013.

Huguet, C., Martens-Habbena, W., Urakawa, H., Stahl, D. A. and Ingalls, A. E.: Comparison of extraction methods for quantitative analysis of core and intact polar glycerol dialkyl glycerol tetraethers (GDGTs) in environmental samples, Limnol. Oceanogr. Methods, 8(APR), 127–145, doi:10.4319/lom.2010.8.127, 2010.

Hurley, S. J., Elling, F. J., Könneke, M., Buchwald, C., Wankel, S. D. and Santoro, A. E.: Influence of ammonia oxidation rate on thaumarchaeal lipid composition and the TEX_{86} temperature proxy, Proc. Natl. Acad. Sci., 113(28), 7762–7767, doi:10.1073/pnas.1518534113, 2016.

Jia, G., Zhang, J., Chen, J., Peng, P. and Zhang, C. L.: Archaeal tetraether lipids record subsurface water temperature in the South China Sea, Org. Geochem., 50, 68–77, doi:10.1016/j.orggeochem.2012.07.002, 2012.

Jia, G., Wang, X., Guo, W. and Dong, L.: Seasonal distribution of archaeal lipids in surface water and its constraint on their sources and the TEX_{86} temperature proxy in sediments of the South China Sea, J. Geophys. Res. Biogeosciences, 122(3), 592–606, doi:10.1002/2016JG003732, 2017.

Kang, S., Shin, K. H. and Kim, J. H.: Occurrence and distribution of hydroxylated isoprenoid glycerol dialkyl glycerol tetraethers (OH-GDGTs) in the Han River system, South Korea, Acta Geochim., 36(3), 367–369, doi:10.1007/s11631-017-0165-3, 2017.

Kim, J. H., Crosta, X., Michel, E., Schouten, S., Duprat, J. and Sinninghe Damsté, J. S.: Impact of lateral transport on organic proxies in the Southern Ocean, Quat. Res., 71(2), 246–250, doi:10.1016/j.yqres.2008.10.005, 2009.

Kim, J. H., van der Meer, J., Schouten, S., Helmke, P., Willmott, V., Sangiorgi, F., Koç, N., Hopmans, E. C. and Damsté, J. S. S.: New indices and calibrations derived from the distribution of crenarchaeal isoprenoid tetraether lipids: Implications for past sea surface temperature reconstructions, Geochim. Cosmochim. Acta, 74(16), 4639–4654, doi:10.1016/j.gca.2010.05.027, 2010.

Kim, J. H., Schouten, S., Rodrigo-Gámiz, M., Rampen, S., Marino, G., Huguet, C., Helmke, P., Buscail, R., Hopmans, E. C., Pross, J., Sangiorgi, F., Middelburg, J. B. M. and Sinninghe Damsté, J. S.: Influence of deep-water derived isoprenoid tetraether lipids on the TEX_{86}^{H} paleothermometer in the Mediterranean Sea, Geochim. Cosmochim. Acta, 150, 125–141, doi:10.1016/j.gca.2014.11.017, 2015.

Kim, J. H., Villanueva, L., Zell, C. and Sinninghe Damsté, J. S.: Biological source and provenance of deep-water derived isoprenoid tetraether lipids along the Portuguese continental margin, Geochim. Cosmochim. Acta, 172, 177–204, doi:10.1016/j.gca.2015.09.010, 2016.

Lattaud, J., Kim, J. H., De Jonge, C., Zell, C., Sinninghe Damsté, J. S. and Schouten, S.: The C_{32} alkane-1,15-diol as a tracer for riverine input in coastal seas, Geochim. Cosmochim. Acta, 202(12), 146–158, doi:10.1016/j.gca.2016.12.030, 2017.

Lincoln, S. A., Wai, B., Eppley, J. M., Church, M. J., Summons, R. E. and DeLong, E. F.: Planktonic Euryarchaeota are a significant source of archaeal tetraether lipids in the ocean, Proc. Natl. Acad. Sci., 111(27), 9858–9863, doi:10.1073/pnas.1409439111, 2014.

Liu, W., Zhang, C. L., Wang, Z., Wang, J., Liu, Z. and Don, H.: Distribution of glycerol dialkyl glycerol tetraethers in surface sediments of Lake Qinghai and surrounding soil, Org. Geochem., 47, 78–87, doi:10.1016/j.orggeochem.2012.03.008, 2012a.

Liu, W. T. and Xie, X.: Space-based observations of the seasonal changes of South Asian monsoons and oceanic responses, Geophys. Res. Lett., 26(10), 1473–1476, doi:10.1029/1999GL900289, 1999.

Liu, X. L., Lipp, J. S., Simpson, J. H., Lin, Y. S., Summons, R. E. and Hinrichs, K. U.: Mono- and dihydroxyl glycerol dibiphytanyl glycerol tetraethers in marine sediments: Identification of both core and intact polar lipid forms, Geochim. Cosmochim. Acta, 89, 102–115, doi:10.1016/j.gca.2012.04.053, 2012b.

Liu, Y., Gao, S., Wang, Y. P., Yang, Y., Long, J., Zhang, Y. and Wu, X.: Distal mud deposits associated with the Pearl River over the northwestern continental shelf of the South China Sea, Mar. Geol., 347, 43–57, doi:10.1016/j.margeo.2013.10.012, 2014.

Lopes Dos Santos, R. A., Spooner, M. I., Barrows, T. T., De Deckker, P., Sinninghe Damsté, J. S. and Schouten, S.: Comparison of organic ($U^{K'}_{37}$, TEX^{H}_{86}, LDI) and faunal proxies (foraminiferal assemblages) for reconstruction of late Quaternary sea surface temperature variability from offshore southeastern Australia, Paleoceanography, 28(3), 377–387, doi:10.1002/palo.20035, 2013.

Lü, X., Yang, H., Song, J., Versteegh, G. J. M., Li, X., Yuan, H., Li, N., Yang, C., Yang, Y., Ding, W. and Xie, S.: Sources and distribution of isoprenoid glycerol dialkyl glycerol tetraethers (GDGTs) in sediments from the east coastal sea of China: Application of GDGT-based paleothermometry to a shallow marginal sea, Org. Geochem., 75, 24–35, doi:10.1016/j.orggeochem.2014.06.007, 2014.

Lü, X., Liu, X. L., Elling, F. J., Yang, H., Xie, S., Song, J., Li, X., Yuan, H., Li, N. and Hinrichs, K. U.: Hydroxylated isoprenoid GDGTs in Chinese coastal seas and their potential as a paleotemperature proxy for mid-to-low latitude marginal seas, Org. Geochem., 89–90, 31–43, doi:10.1016/j.orggeochem.2015.10.004, 2015.

Lü, X., Chen, J., Han, T., Yang, H., Wu, W., Ding, W. and Hinrichs, K. U.: Origin of hydroxyl GDGTs and regular isoprenoid GDGTs in suspended particulate matter of Yangtze River Estuary, Org. Geochem., 128, 78–85, doi:10.1016/j.orggeochem.2018.12.010, 2019.

Lu, Z. and Gan, J.: Controls of seasonal variability of phytoplankton blooms in the Pearl River Estuary, Deep. Res. Part II Top. Stud. Oceanogr., 117, 86–96, doi:10.1016/ j.dsr2.2013.12.011, 2015.

Müller, P. J. and Fischer, G.: C_{37}-Alkenones as paleotemperature tool: fundamentals based on sediment traps and surface sediments from the South Atlantic Ocean [M], The South Atlantic in the late Quaternary, Springer, Berlin, Heidelberg, 167–193, doi:10.1007/978-3-642-18917-3, 2003.

Müller, P. J., Kirst, G., Ruhland, G., Von Storch, I. and Rosell-Melé, A.: Calibration of the alkenone paleotemperature index $U^{K'}_{37}$ based on core-tops from the eastern South Atlantic and the global ocean (60° N–60° S), Geochim. Cosmochim. Acta, 62(10), 1757–1772, 10.1016/S0016-7037(98)00097-0, 1998.

Paasche, E.: A review of the coccolithophorid *Emiliania huxleyi* (*Prymnesiophyceae*), with particular reference to growth, coccolith formation, and calcification-photosynthesis interactions, Phycologia, 40(6), 503–529, doi:10.2216/i0031-8884-40-6-503.1, 2010.

Park, E., Hefter, J., Fischer, G., Hvitfeldt Iversen, M., Ramondenc, S., Nthig, E. M. and Mollenhauer, G.: Seasonality of archaeal lipid flux and GDGT-based thermometry in sinking particles of high-latitude oceans: Fram Strait (79° N) and Antarctic Polar Front (50° S), Biogeosciences, 16(11), 2247–2268, doi:10.5194/bg-16-2247-2019, 2019.

Pelejero, C. and Grimalt, J. O.: The correlation between the $U^{K'}_{37}$ index and sea surface temperatures in the warm boundary: The South China Sea, Geochim. Cosmochim. Acta, 61(22), 4789–4797, doi:10.1016/S0016-7037(97)00280-9, 1997.

Prahl, F. G., Muehlhausen, L. A. and Zahnle, D. L.: Further evaluation of long-chain alkenones as indicators of

paleoceanographic conditions, Geochim. Cosmochim. Acta, 52(9), 2303–2310, doi:10.1016/0016-7037(88)90132-9, 1988.

Prahl, F. G., Sparrow, M. A. and Wolfe, G. V.: Physiological impacts on alkenone paleothermometry, Paleoceanography, 18(2), doi:10.1029/2002pa000803, 2003.

Prahl, F. G. and Wakeham, S. G.: Calibration of unsaturation patterns in long-chain ketone compositions for palaeotemperature assessment, Nature, 330(6146), 367, 1987.

Rampen, S. W., Schouten, S. and Wakeham, S. G.: Seasonal and spatial variation in the sources and fluxes of long chain diols and mid-chain hydroxy methyl alkanoates in the Arabian Sea, , 38, 165–179, doi:10.1016/j.orggeochem.2006.10.008, 2007.

Rampen, S. W., Willmott, V., Kim, J. H., Uliana, E., Mollenhauer, G., Schefuß, E., Sinninghe Damsté, J. S. and Schouten, S.: Long chain 1,13- and 1,15-diols as a potential proxy for palaeotemperature reconstruction, Geochim. Cosmochim. Acta, 84, 204–216, doi:10.1016/j.gca.2012.01.024, 2012.

Rampen, S. W., Willmott, V., Kim, J., Rodrigo-gámiz, M., Uliana, E., Mollenhauer, G., Schefuß, E., Sinninghe, J. S. and Schouten, S.: Organic Geochemistry Evaluation of long chain 1,14-alkyl diols in marine sediments as indicators for upwelling and temperature, Org. Geochem., 76, 39–47, doi:10.1016/j.orggeochem.2014.07.012, 2014a.

Rampen, S. W., Datema, M., Rodrigo-Gamiz, M., Schouten, S., Reichart, G. and Damste, J. S. S.: Sources and proxy potential of long chain alkyl diols in lacustrine environments, Geochim. Cosmochim. Acta,144, 59–71, doi:10.1016/j.gca.2014.08.033, 2014b.

Riegman, R., Noordeloos, A. A. M. and Cadée, G. C.: *Phaeocystis* blooms and eutrophication of the continental coastal zones of the North Sea, Mar. Biol., 112(3), 479–484, doi:10.1007/BF00356293, 1992.

Rosell-Melé, A. and Prahl, F. G.: Seasonality of $U_{37}^{K'}$ temperature estimates as inferred from sediment trap data, Quat. Sci. Rev., 72, 128–136, doi:10.1016/j.quascirev.2013.04.017, 2013.

Sawada, K., Handa, N., Shiraiwa, Y., Danbara, A. and Montani, S.: Long-chain alkenones and alkyl alkenoates in the coastal and pelagic sediments of the northwest north Pacific, with special reference to the reconstruction of Emiliania huxleyi and Gephyrocapsa oceanica ratios, Org. Geochem., 24(8–9), 751–764, doi:10.1016/S0146-6380(96)00087-3, 1996.

Schouten, S., Hopmans, E. C., Schefuß, E. and Sinninghe Damsté, J. S.: Distributional variations in marine crenarchaeotal membrane lipids: a new tool for reconstructing ancient sea water temperatures? Earth Planet. Sci. Lett., 204(1–2), 265–274, 2002.

Schouten, S., Hopmans, E. C. and Sinninghe Damsté, J. S.: The organic geochemistry of glycerol dialkyl glycerol tetraether lipids: A review, Org. Geochem., 54, 19–61, doi:10.1016/j.orggeochem.2012.09.006, 2013.

Sinninghe Damsté, J. S., Rijpstra, W. I. C., Hopmans, E. C., Jung, M. Y., Kim, J. G., Rhee, S. K., Stieglmeier, M. and Schleper, C.: Intact polar and core glycerol dibiphytanyl glycerol tetraether lipids of group I.1a and I.1b Thaumarchaeota in soil, Appl. Environ. Microbiol., 78(19), 6866–6874, doi:10.1128/AEM.01681-12, 2012.

Smith, M., Deckker, P. De, Rogers, J., Brocks, J., Hope, J., Schmidt, S., Lopes, R. and Schouten, S.: Comparison of $U_{37}^{K'}$, TEX_{86}^{H} and LDI temperature proxies for reconstruction of south-east Australian ocean temperatures, Org. Geochem., 64,

94–104, doi:10.1016/j.org-geochem.2013.08.015, 2013.

Sonzogni, C., Bard, E., Rostek, F., Dollfus, D., Rosell-Melé, A., and Eglinton, G.: Temperature and Salinity Effects on Alkenone Ratios Measured in Surface Sediments from the Indian Ocean, Quat. Res., 47(3), 344–355. doi:10.1006/qres.1997.1885, 1997.

Su, J.: Overview of the South China Sea circulation and its influence on the coastal physical oceanography outside the Pearl River Estuary, Cont. Shelf Res., 24(16), 1745–1760, doi:10.1016/j.csr.2004.06.005, 2004.

Tierney, J. E. and Tingley, M. P.: A Bayesian, spatially-varying calibration model for the TEX_{86} proxy, Geochim. Cosmochim. Acta, 127, 83–106, doi:10.1016/j.gca.2013.11.026, 2014.

Tierney, J. E. and Tingley, M. P.: BAYSPLINE: A New Calibration for the Alkenone Paleothermometer, Paleoceanogr. Paleoclimatology, 33(3), 281–301, doi:10.1002/2017PA-003201, 2018.

Taylor, K. W. R., Huber, M., Hollis, C. J., Hernandez-Sanchez, M. T. and Pancost, R. D.: Re-evaluating modern and Palaeogene GDGT distributions: Implications for SST reconstructions, Glob. Planet. Change, 108, 158–174, doi:10.1016/j.gloplacha.2013.06.011, 2013.

Tyrrell, T. and Taylor, A. H.: A modelling study of *Emiliania huxleyi* in the NE atlantic, J. Mar. Syst., 9(1–2), 83–112, doi:10.1016/0924-7963(96)00019-X, 1996.

Turich, C., Freeman, K. H., Bruns, M. A., Conte, M., Jones, A. D. and Wakeham, S. G.: Lipids of marine Archaea: Patterns and provenance in the water-column and sediments, Geochim. Cosmochim. Acta, 71(13), 3272–3291, doi:10.1016/j.gca.2007.04.013, 2007.

Villanueva, L., Schouten, S. and Sinninghe Damsté, J. S.: Depth-related distribution of a key gene of the tetraether lipid biosynthetic pathway in marine Thaumarchaeota, Environ. Microbiol., 17(10), 3527–3539, doi:10.1111/1462-2920.12508, 2015.

Versteegh, G. J. M. and Leeuw, J. W. D. E.: Potential palaeoenvironmental information of C_{24} to C_{36} mid-chain diols, keto-ols and mid-chain hydroxy fatty acids; a critical review, Org. Geochem., 27(97), 1–13, https://doi.org/10.1016/S0146-6380(97)00063-6, 1997.

Versteegh, G. J. M., Riegman, R., Leeuw, J. W. De and Jansen, J. H. F. F.: $U_{37}^{K'}$ values for Isochrysis galbana as a function of culture temperature, light intensity and nutrient concentrations, Org. Geochem., 32, 785–794, doi:10.1016/S0146-6380(01)00041-9, 2001.

Volkman J. K., Barrett, S. M., Blackburn S. I., Sikes, E. L.: Alkenones in *Gephyrocapsa oceanica*: Implications for studies of paleoclimate, Geochim. Cosmochim. Acta, 59(3), 513–520, doi:10.1016/0016-7037(95)00325-T, 1995.

Volkman, J. K., Barrett, S. M., Blackburn, S. I.: Eustigmatophyte microalgae are potential sources of C_{29} sterols, C_{22}–C_{28} n-alcohols and C_{28}–C_{32} n-alkyl diols in freshwater environments, Org. Geochem., 30(5): 307–318, doi:10.1016/S01466380(99)00009-1, 1999.

Wang, J. X., Wei, Y., Wang, P., Hong, Y. and Zhang, C. L.: Unusually low TEX_{86} values in the transitional zone between Pearl River estuary and coastal South China Sea: Impact of changing archaeal community composition, Chem. Geol., 402,

18–29, doi:10.1016/j.chem-geo.2015.03.002, 2015.

Wei, Y., Wang, J., Liu, J., Dong, L., Li, L., Wang, H., Wang, P., Zhao, M. and Zhang, C. L.: Spatial variations in archaeal lipids of surface water and core-top sediments in the South China Sea and their implications for paleoclimate studies, Appl. Environ. Microbiol., 77(21), 7479–7489, doi:10.1128/AEM.00580-11, 2011.

Weijers, J. W. H., Schouten, S., Spaargaren, O. C. and Sinninghe Damsté, J. S.: Occurrence and distribution of tetraether membrane lipids in soils: Implications for the use of the TEX_{86} proxy and the BIT index, Org. Geochem., 37(12), 1680–1693, doi:10.1016/j.orggeochem.-2006.07.018, 2006.

Weijers, J. W. H., Lim, K. L. H., Aquilina, A., Damsté, J. S. S. and Pancost, R. D.: Biogeochemical controls on glycerol dialkyl glycerol tetraether lipid distributions in sediments characterized by diffusive methane flux, Geochemistry, Geophys. Geosystems, 12(10), 1–15, doi:10.1029/2011GC003724, 2011.

Wong, G. T. F., Pan, X., Li, K. Y., Shiah, F. K., Ho, T. Y. and Guo, X.: Hydrography and nutrient dynamics in the Northern South China Sea Shelf-sea (NoSoCS), Deep. Res. Part II: Top. Stud. Oceanogr., 117, 23–40, doi:10.1016/j.dsr2.2015.02.023, 2015.

Xie, W., Zhang, C., Zhou, X. and Wang, P.: Salinity-dominated change in community structure and ecological function of Archaea from the lower Pearl River to coastal South China Sea, Appl. Microbiol. Biotechnol., 98(18), 7971–7982, doi:10.1007/s00253-014-5838-9, 2014.

Xu, J., Yin, K., He, L., Yuan, X., Ho, A. Y. T. and Harrison, P. J.: Phosphorus limitation in the northern South China Sea during late summer: Influence of the Pearl River, Deep. Res. Part I: Oceanogr. Res. Pap., 55(10), 1330–1342, doi:10.1016/j.dsr.2008.05.007, 2008.

Yang, Y., Gao, C., Dang, X., Ruan, X., Lü, X., Xie, S., Li, X., Yao, Y. and Yang, H.: Assessing hydroxylated isoprenoid GDGTs as a paleothermometer for the tropical South China Sea, Org. Geochem., 115, 156–165, doi:10.1016/j.orggeochem.2017.10.014, 2018.

Zhang, C. L., Wang, J., Wei, Y., Zhu, C., Huang, L. and Dong, H.: Production of branched tetraether lipids in the lower Pearl River and estuary: Effects of extraction methods and impact on bGDGT proxies, Front. Microbiol., 2(JAN), 1–18, doi:10.3389/fmicb.2011.00274, 2012.

Zhang, J., Bai, Y., Xu, S., Lei, F. and Jia, G.: Alkenone and tetraether lipids reflect different seasonal seawater temperatures in the coastal northern South China Sea, Org. Geochem., 58, 115–120, doi:10.1016/j.orggeochem.2013.02.012, 2013.

Zhang, J., Jia, G., Guo, W., Wang, X. and Lei, F.: Isoprenoid tetraether lipids in suspended particulate matter from the East China Sea and implication for sedimentary records, Org. Geochem., 114, 81–90, doi:10.1016/j.orggeochem.2017.09.006, 2017.

Zhang, Y. G., Pagani, M. and Wang, Z.: Ring Index: A new strategy to evaluate the integrity of TEX_{86} paleothermometry, Paleoceanography, 31(2), 220–232, doi:10.1002/2015PA002848, 2016.

Zhang, Y. G., Zhang, C. L., Liu, X. L., Li, L., Hinrichs, K. U. and Noakes, J. E.: Methane Index: A tetraether archaeal lipid biomarker indicator for detecting the instability of marine gas hydrates, Earth Planet. Sci. Lett., 307(3–4), 525–534,

doi:10.1016/j.epsl.2011.05.031, 2011.

Zhu, C., Weijers, J. W. H., Wagner, T., Pan, J. M., Chen, J. F. and Pancost, R. D.: Sources and distributions of tetraether lipids in surface sediments across a large river-dominated continental margin, Org. Geochem., 42(4), 376–386, doi:10.1016/j.orggeochem.2011.02.002, 2011.

Zhou, H., Hu, J., Spiro, B., Peng, P. and Tang, J.: Glycerol dialkyl glycerol tetraethers in surficial coastal and open marine sediments around China: Indicators of sea surface temperature and effects of their sources, Palaeogeogr. Palaeoclimatol. Palaeoecol., 395, 114–121, doi:10.1016/j.palaeo.2013.12.006, 2014.

Zhu, X., Mao, S., Wu, N., Sun, Y. and Guan, H.: Molecular and stable carbon isotopic compositions of saturated fatty acids within one sedimentary profile in the Shenhu, northern South China Sea: Source implications, J. Asian Earth Sci., 92, 262–275, doi:10.1016/j.jseaes.2013.12.011, 2014.

Zhu, X., Jia, G., Mao, S. and Yan, W.: Sediment records of long chain alkyl diols in an upwelling area of the coastal northern South China Sea, Org. Geochem., 121, 1–9, doi:10.1016/j.orggeochem.2018.03.014, 2018.

Table 1: Sampling sites, SST and proxy values from the PRE and northern SCS shelf (water depth (WD), sea surface temperature (SST) obtained from WOA18, RI-OH, ring index of OH-GDGTs).

Sites	Latitude (°N)	Longitude (°E)	WD (m)	SST_{annual} (°C)	SST_{winter} (°C)	SST_{spring} (°C)	SST_{summer} (°C)	SST_{autumn} (°C)	$U^{K'}_{37}$	LDI	TEX_{86}	TEX^{H}_{86}	BIT	RI-OH
PRE-Y6	22.3	113.8	6.5	25.2	20.9	25.4	29.0	25.4	0.91	0.69	0.53	-0.28	0.28	1.69
PRE-Y11	22.1	113.7	8.0	25.2	20.9	26.3	29.0	25.7	0.91	0.81	0.56	-0.25	0.16	1.72
SXCB	21.5	112.7	14	25.7	21.7	25.8	28.9	25.2	0.90	0.90	0.49	-0.31	0.15	1.62
GLB	21.7	113.0	15	25.2	21.0	25.4	29.0	25.4	0.90	0.86	0.50	-0.30	0.19	1.62
PRE-A8	22.7	113.7	17.5	25.2	20.9	25.0	28.7	24.8	0.81	0.56	0.60	-0.22	0.49	1.79
QD00	21.1	110.8	18	24.2	18.2	25.4	29.0	25.4	0.88	0.93	0.48	-0.31	0.07	1.61
LD-GSD	22.1	113.8	21	25.2	20.9	25.5	28.9	25.4	0.91	--	0.57	-0.24	0.28	--
WSB	22.0	113.7	21	25.2	21.0	26.2	28.7	25.1	0.91	0.93	0.55	-0.26	0.25	--
MMDB	21.2	111.3	26	24.9	19.7	26.3	29.0	25.6	0.85	0.64	0.47	-0.33	0.10	1.59
E700	21.5	112.5	26	25.6	21.5	26.3	29.0	25.7	0.93	0.94	0.48	-0.32	0.08	1.60
YJXB	21.4	111.8	27	25.7	21.7	26.0	28.9	25.2	0.89	0.94	0.55	-0.26	0.22	--
E600	21.3	111.7	29	25.0	19.9	25.5	29.0	25.4	0.93	0.95	0.49	-0.31	0.05	1.60
A9	22.0	114.0	35	25.2	21.1	26.3	29.0	25.7	0.92	0.93	0.49	-0.31	0.06	1.58
E701	21.2	112.7	45	25.7	21.7	27.0	28.5	25.7	0.93	0.95	0.53	-0.27	0.06	1.63
QD04	20.4	111.1	47	25.7	21.6	25.8	29.0	25.6	0.91	0.94	0.49	-0.31	0.06	1.57
SW10	22.1	115.0	58	25.6	22.2	26.5	28.9	26.0	0.93	0.97	0.54	-0.27	0.04	1.66
LD-11	20.9	114.5	86	26.2	23.2	26.2	28.9	25.8	0.94	0.97	0.60	-0.22	0.02	1.73
A6	21.3	114.7	88	25.9	22.7	26.8	29.0	26.2	0.94	0.97	0.56	-0.25	0.05	1.65
LD-18	20.6	113.8	88	26.2	22.9	26.7	29.0	26.0	0.92	0.98	0.60	-0.22	0.03	1.73
QD11a	20.7	113.4	90	26.1	22.5	27.2	29.1	25.9	0.92	0.95	0.51	-0.29	0.06	1.61
QD41	20.1	112.1	90	26.2	22.4	28.0	29.4	26.2	0.91	0.97	0.59	-0.23	0.03	1.68
E503	19.2	112.3	186	26.8	23.7	28.0	29.1	26.6	0.94	0.98	0.65	-0.19	0.03	1.72
LD-21	19.7	114.6	1307	27.0	24.1	25.4	29.0	25.4	0.94	0.98	0.65	-0.18	0.03	1.64

730 **Table 2: Pearson correlation coefficient analysis of different diols in surface sediments in this study.**

Pearson correlation coefficient	C_{28} 1,13-diol	C_{30} 1,13-diol	C_{30} 1,15-diol	C_{32} 1,15-diol
C_{28} 1,13-diol	1			
C_{30} 1,13-diol	0.83**	1		
C_{30} 1,15-diol	−0.68**	−0.90**	1	
C_{32} 1,15-diol	0.56**	0.78**	−0.90**	1

**** $p < 0.005$**

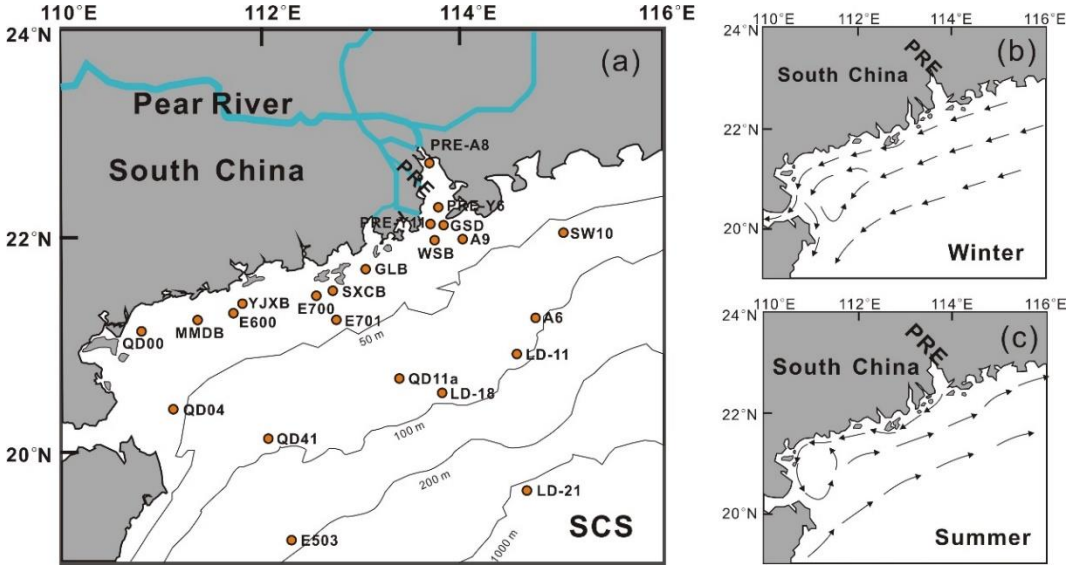

Figure 1: (a) Sampling sites and patterns of the surface coastal currents in (b) winter and (c) summer, respectively (modified from Liu et al. (2014)).

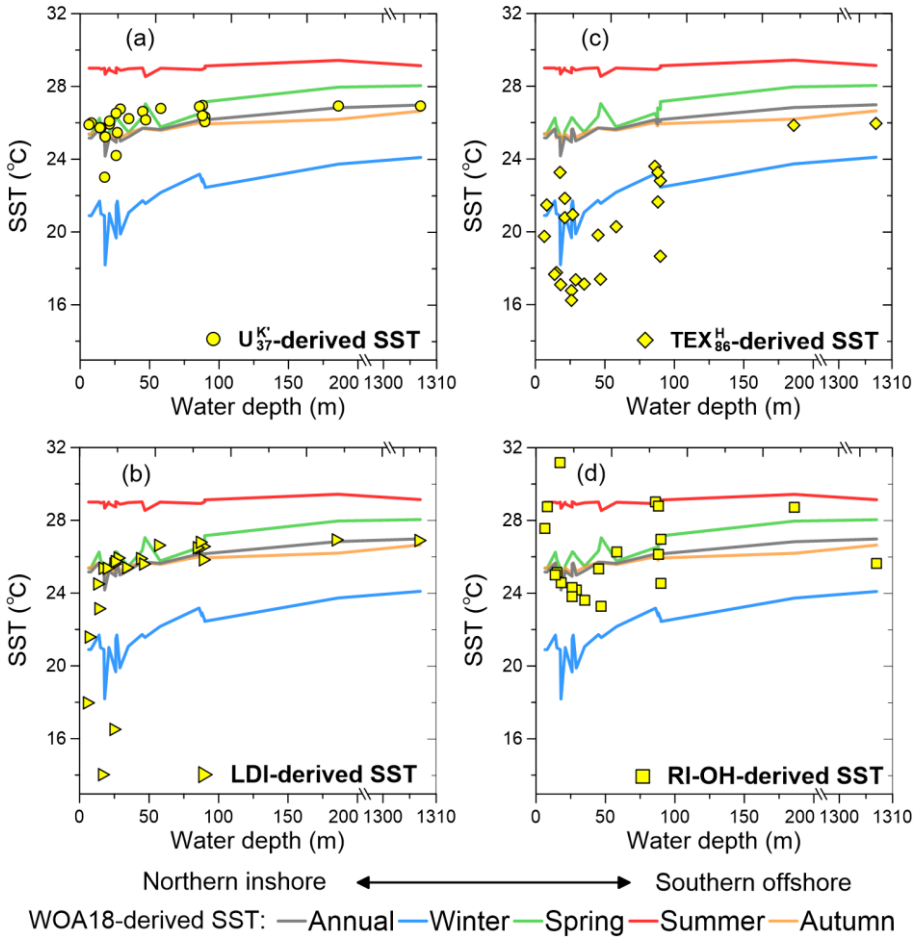

735

Figure 2: Changes with water depth of WOA-derived and proxy-derived SSTs for: (a) $U^{K'}_{37}$, (b) LDI, (c) TEX^{H}_{86}, and (d) RI-OH.

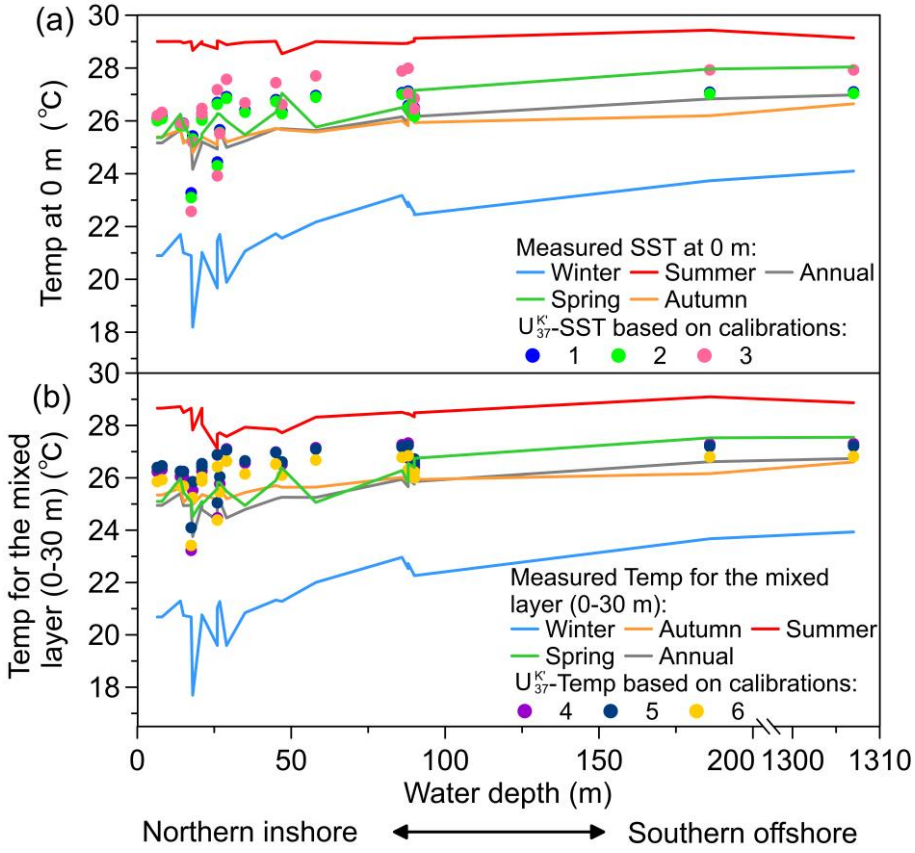

Figure 3: (a) A comparison between $U^{K'}_{37}$-SST values calculated using different calibrations and the measured annual/seasonal SST (0 m). Calibrations were based on: (1) Müller et al., 1998; (2) Müller and Fischer, 2003; (3) BAYSPLINE (Tierney and Tingley, 2018); (b) A comparison between $U^{K'}_{37}$-SST values calculated using different calibrations and the measured annual/seasonal SST for the mixed layers (0-30 m). Calibrations were applied to (4) the SCS (Pelejero and Grimalt, 1997); (5) the Pacific Ocean (Conte et al., 2006); (6) the global Oceans (Conte et al., 2006).

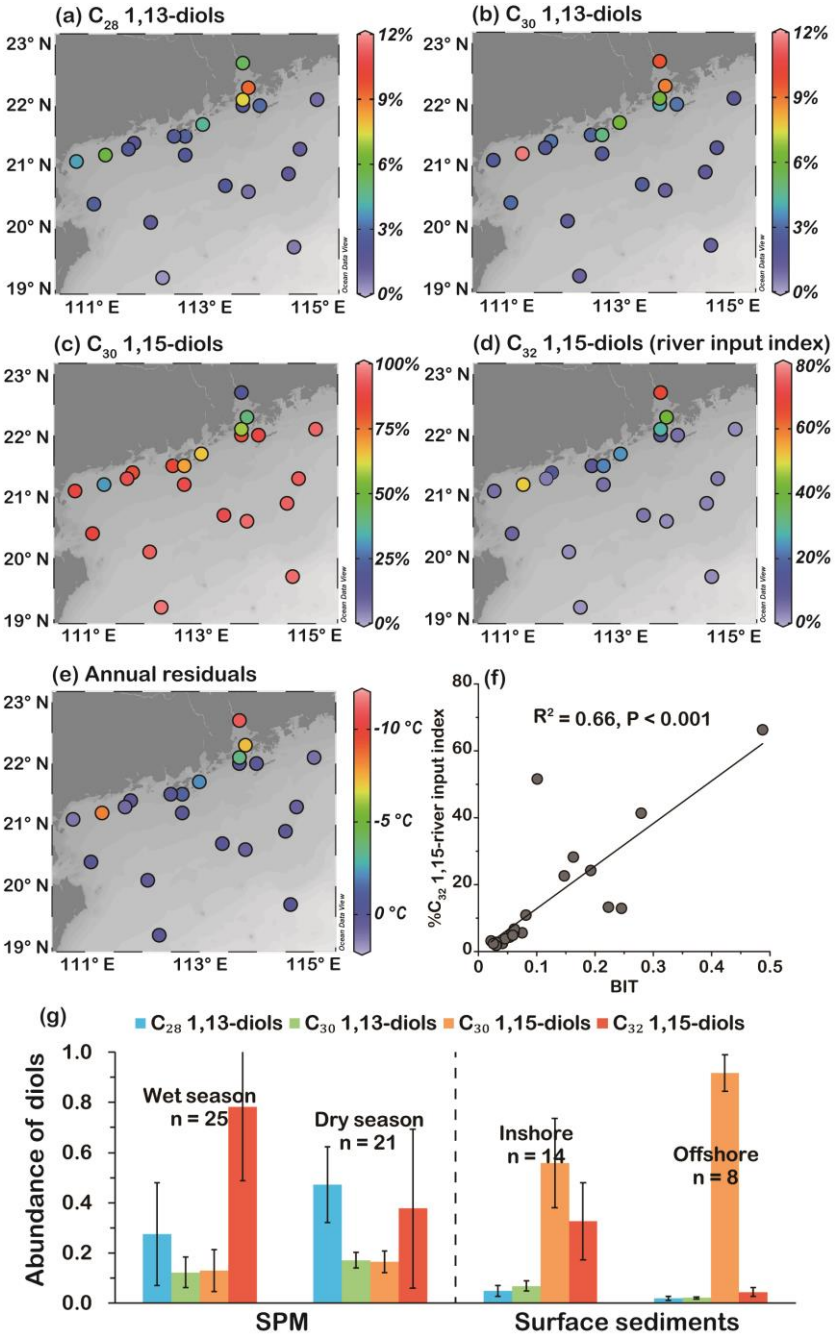

745

Figure 4: Distribution of relative abundances of: (a) C_{28} 1,13-diol, (b) C_{30} 1,13-diol, (c) C_{30} 1,15-diol, and (d) C_{32} 1,15-diol (river input index); (e) Distribution of annual residuals (LDI-derived SST minus observed annual SST from WOA18); (f) Relationship between BIT and %C_{32} 1,15 (river input index) (curve shows linear fit); (g) Distribution of average diol abundance in SPM in the PRE (data from Zhu et al. (2018)), inshore and offshore surface sediments (data from this study) (Error bars indicate the standard

750 **deviations).**

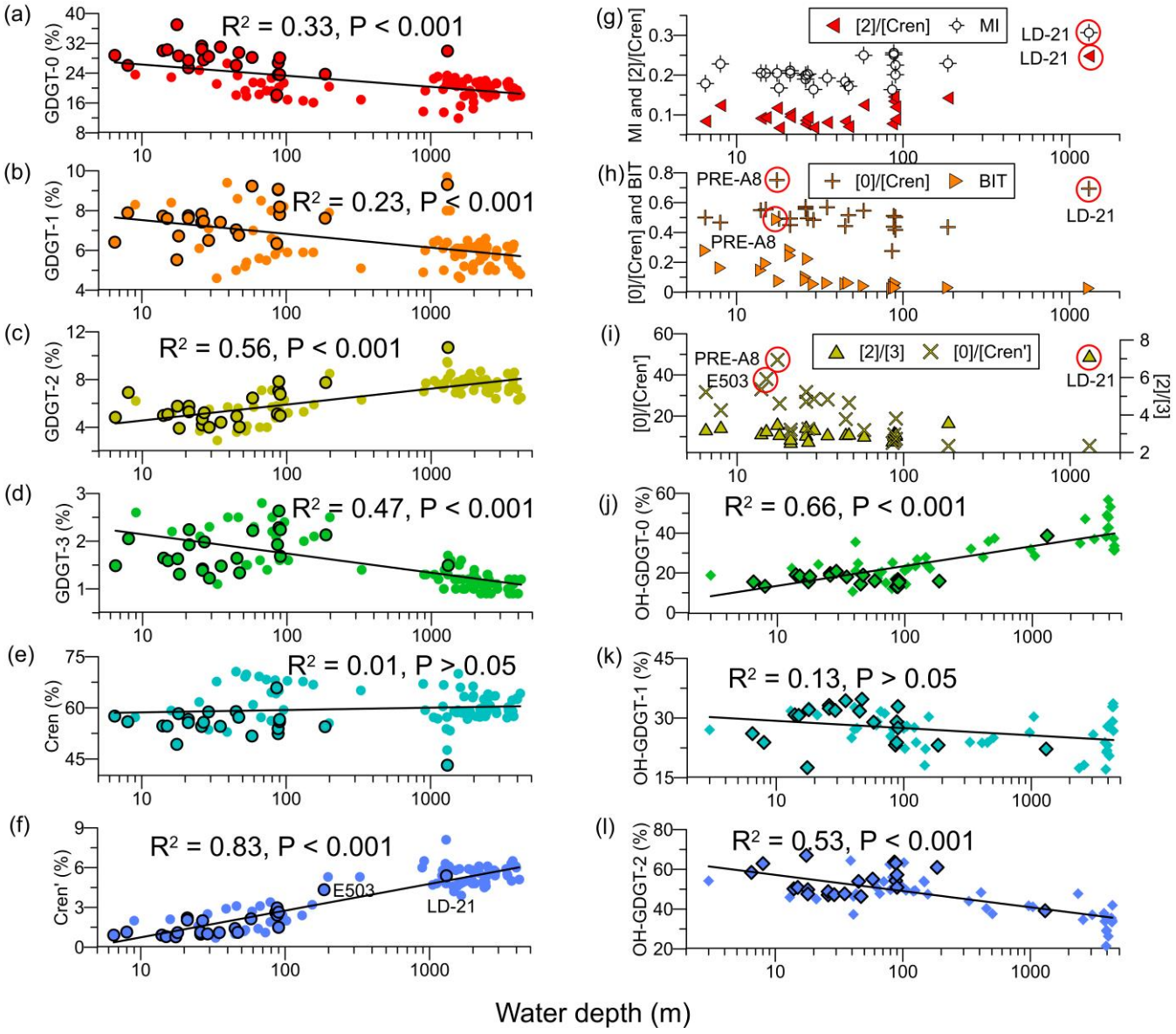

Figure 5: Depth profiles of the relative abundance of individual iGDGTs: (a) GDGT-0, (b) GDGT-1, (c) GDGT-2, (d) GDGT-3, (e) Cren, and (f) Cren' (dots with black marks from this study and without black marks from Ge et al. (2013), Jia et al. (2017), Wei et al. (2011), and Zhou et al. (2014); Black curves show lognormal fits for all surface sediments data in the SCS). Depth profiles of (g) [2]/[Cren] ratio and MI values, (h) [0]/[Cren] ratio and BIT values, and (i) [2]/[3] and [0]/[Cren']ratios. Depth profiles of the relative abundance of individual OH-GDGTs: (j) OH-GDGT-0, (k) OH-GDGT-1, and (l) OH-GDGT-2 (dots with black marks from this study and without black marks from Lü et al. (2015) and Yang et al. (2018); Black curves show lognormal fits for all surface sediments data in the SCS).

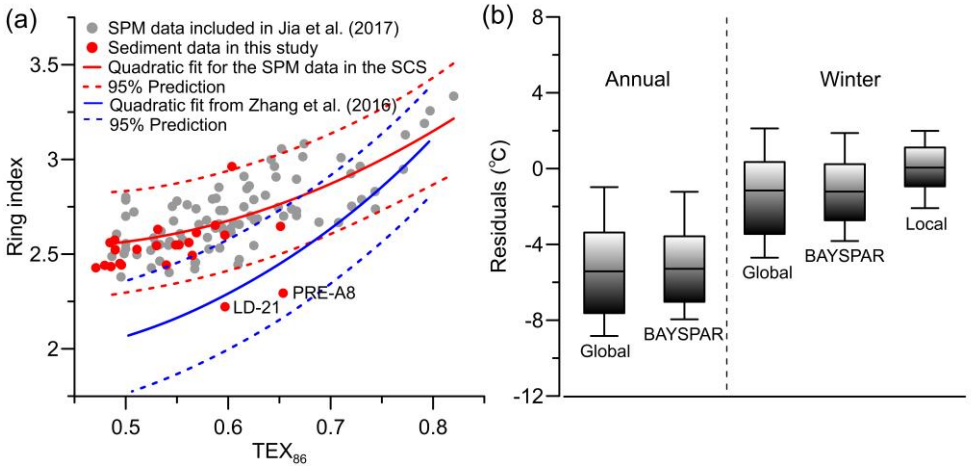

Figure 6: (a) Ring index-TEX_{86} crossplots for surface sediments in this study (red dots) and surface water SPM from Jia et al. (2017) (grey dots). Red curve is the quadratic fit for the SPM data in the SCS while blue curve have been presented by Zhang et al. (2016) for the global sediment data. Dashed curves are the 95% prediction limits for the quadratic fit; (b) Box-Whisker plot of annual residuals based on the global calibration (Kim et al., 2010) and BAYSPAR (Tierney and Tingley, 2014), as well as winter residuals based on the global calibration (Kim et al., 2010), BAYSPAR (Tierney and Tingley, 2014), and local calibration from winter SPM (Jia et al., 2017).

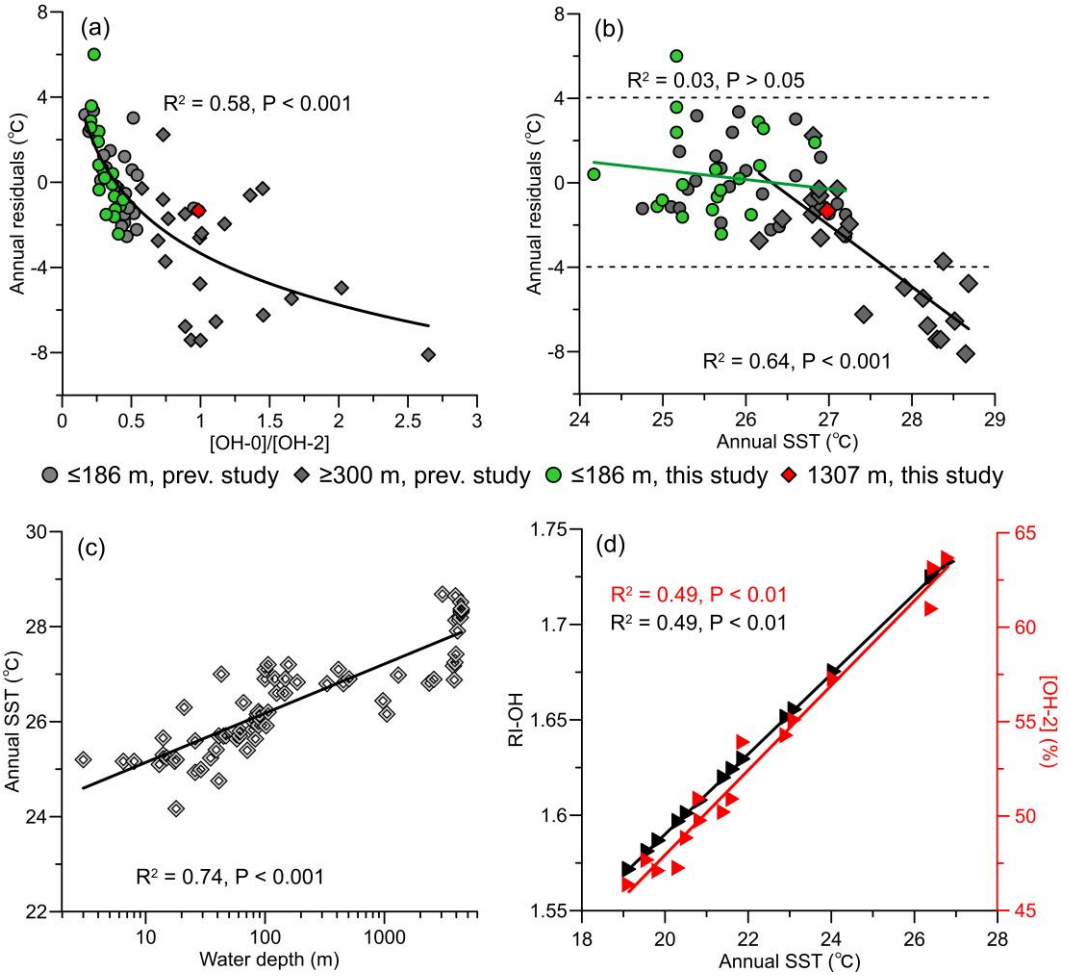

Figure 7: Changes of annual residuals with (a) [OH-0]/[OH-2] ratios (black curve is the lognormal fit for the surface sediment data in the SCS), and (b) annual SST; (Green and black curves are linear fits for "shallow-water" and "deep-water" samples in the SCS, respectively, and annual residuals are RI-OH-derived SSTs minus observed annual SSTs from WOA18; Previous study in (a) and (b) includes Lü et al. (2015) and Yang et al. (2018)); Relationship of (c) RI-OH with annual and seasonal SSTs for data from this study, Lü et al. (2015) and Yang et al. (2018) (black curve is lognormal fit), (d) Annual SST with RI-OH and [OH-2] for data in this study (red and black curves are linear fits).